Tropical Cyclone Formation

MICHAEL T. MONTGOMERY* AND BRIAN F. FARRELL

Department of Earth and Planetary Sciences, Harvard University, Cambridge, Massachusetts

(Manuscript received 25 October 1991, in final form 20 April 1992)

ABSTRACT

The physics of tropical cyclone formation is not well understood, and more is known about the mature hurricane than the formative mechanisms that produce it. It is believed part of the reason for this can be traced to insufficient upper-level atmospheric data. Recent observations suggest that tropical cyclones are initiated by asymmetric interactions associated with migratory upper-level potential vorticity disturbances and low-level disturbances. Favored theories of cyclone formation, however, focus on internal processes associated with cumulus convection and/or air–sea interaction. This work focuses on external mechanisms of cyclone formation and, using both a two- and three-dimensional moist geostrophic momentum model, investigates the role of upper-level potential vorticity disturbances on the formation process.

A conceptual model of tropical cyclone formation is proposed, and implications of the theory are discussed.

1. Introduction

Tropical cyclones are large-scale rotary storms that form over warm ocean waters in tropical regions, and their outer circulations can extend more than 1000 km from the storm center. The mature tropical cyclone (called a hurricane in the Atlantic and a typhoon in the Pacific), possesses sustained surface winds of 33 m s^{-1} or higher, and represents the most intense phase in the tropical cyclone life cycle. Its extremely high winds, torrential rainfall, and storm surge make the hurricane one of the most life threatening and destructive natural phenomena on earth. The less intense tropical cyclones are called tropical depressions (rotary winds less than 17 m s^{-1}) and tropical storms (rotary winds less than 33 m s^{-1}), but they too carry destructive potential and are frequently associated with heavy precipitation. Surprisingly little is known about how tropical cyclones form (Frank 1987). There is limited data over the oceans where the formation process occurs, and a widely accepted model of tropical cyclone formation (defined here as the transformation from a tropical disturbance to a tropical cyclone, and used interchangeably with genesis throughout) does not yet exist.

In the absence of reliable forecast capability, priority has been given to providing sufficient warning to inhabited coastal areas by predicting the track of the mature tropical cyclone (Elsberry 1987; Elsberry and Abbey 1991). The problem of predicting the time and location of cyclone formation has proven to be more difficult, and understanding the physics of tropical cyclone formation remains a central problem in meteorology and atmospheric forecast.

It is widely accepted that tropical cyclones form in moist unstable environments in association with low-level tropical disturbances (such as easterly waves, or tropical cloud clusters) and warm sea surface temperatures, though only a very small percentage of these disturbances evolve into tropical cyclones. For example, during the warmer months in the North Atlantic, at least one westward-moving disturbance is present every day, but an average of only eight disturbances per year become tropical storms, and about 60% of these achieve hurricane strength (Palmen and Newton 1969). Thus, a tropical disturbance that somehow has been transformed into a tropical storm will likely intensify into a hurricane, but the factors responsible for the transformation of a tropical disturbance into a tropical storm, and ultimately into a full-fledged hurricane, are poorly understood.

Tropical cyclones are considered to form by a process completely different from that responsible for midlatitude cyclone formation. Midlatitude cyclones form by extracting available potential energy stored in areas of strong baroclinicity. Baroclinic dynamics is believed unimportant in tropical cyclone formation since surface temperature gradients in the tropics are small and much of the tropical atmosphere does not support baroclinic instabilities. Rather, the heat of condensation and the convective available potential energy (CAPE) in moist convective cloud systems appears to be the primary hurricane energy source. Tropical cyclones

* Present affiliation: Department of Atmospheric Sciences, Colorado State University.

Corresponding author address: Dr. Michael T. Montgomery, Department of Atmospheric Sciences, Colorado State University, Fort Collins, CO 80523.

were thus originally viewed as large-scale instabilities associated with conditionally unstable tropical air.

Early theoretical work focused on conditional instabilities of a quiescent atmosphere in a rapidly rotating environment, but failed to find rotary instabilities with scales comparable to tropical cyclones. Indeed, linear convective models favored the smallest cumulus scales (Haque 1952; Lilly 1960; and others). A new type of instability, called conditional instability of the second kind (CISK), was then proposed to explain the growth of the tropical depression (Charney and Eliassen 1964; Ooyama 1964). In CISK, tropical depressions intensify by utilizing the CAPE through a cooperative feedback between cumulus clouds and the large-scale flow. For suitable parameter values, linear CISK predicts large-scale amplifying disturbances with *e*-folding times on the order of a few days. A shortfall of linearized CISK theory, however, is that the exponential growth rate is sensitive to the parameterized vertical heating distribution representing the cumulus ensemble. Depending upon model assumptions, growth rates may diverge for the smaller scales (Pederson and Rasmussen 1985; Pederson 1991).

As noted by Ooyama (1982), the CISK acronym in common usage today no longer conveys a clear meaning. Physically speaking, the CISK closure is only valid after an incipient vortex has attained sufficient strength and organization so that the cloud-organizing mesoscales are correlated with the balanced flow. The CISK closure is invalid in the early stage of the tropical cyclone since the characteristic scales of the convective clouds and the balanced flow (the latter defined by the internal deformation radius) are so disparate, and was never intended for inquiry into the question of tropical cyclogenesis (Ooyama 1982). Hence, while most analytical demonstrations of CISK are linear, the results should only be interpreted physically as describing storm intensification starting from an already well-developed circulation. An analytical CISK theory that investigates such threshold behavior has been developed recently by Handel (1990). In this work, CISK will generically be regarded as a cooperative intensification process.

Recently, air–sea interaction theory has been proposed as an alternative to CISK (Rotunno and Emanuel 1987; Emanuel 1991). This theory emphasizes augmented latent and sensible heat sea-to-air transfer above ambient values, but also requires sufficiently well-developed axisymmetric disturbances to initiate the air–sea interaction intensification process. Thus, both CISK and air–sea interaction implicitly assume that the transformation from a tropical disturbance to a finite-amplitude rotary system has already taken place, while the processes that produce such initial flow configurations are not addressed in either theory.

A different theoretical approach to the tropical cyclogenesis problem focuses on the effects of eddy angular momentum fluxes associated with upper-level wave asymmetries in the environment of tropical disturbances. While the importance of eddy angular momentum fluxes in the mature hurricane environment was suggested long ago by Pfeffer (1955, 1958), observations suggest that upper-level asymmetries may also be important in cyclogenesis. Using a three-dimensional primitive equation model with cloud physics, Challa and Pfeffer (1990) illustrate rapid hurricane development in cases of strong eddy momentum flux convergence toward the storm center. In this approach, tropical cyclones are viewed to form efficiently in conjunction with cumulus convection and external forcing by upper-level wave asymmetries rather than from solely internal cooperative processes between cumulus convection and frictional convergence in the boundary layer.

Observations of tropical cyclone formation in the western North Atlantic basin suggest that a juxtaposition between a westerly moving upper-level trough, and an easterly moving low-level tropical disturbance is associated with spinup of a tropical storm (Riehl 1948, 1979; Erickson 1967; Yanai 1968; Hawkins and Rubsam 1968; Bosart and Bartlo 1991; Reilly and Emanuel 1991; J. Molinari 1991, personal communication). The majority of these storms supported by upper-level disturbances develop, sometimes quite rapidly, into hurricanes at later times. Observations during the Australian Monsoon Experiment (AMEX) document the formation and structure of tropical cyclones Irma and Jason, which developed over the Gulf of Carpentaria in northern Australia and evolved almost entirely within the experiment's observing network (Davidson et al. 1990). This work suggests that both Irma and Jason formed in association with an equatorward-moving tropical upper-tropospheric trough (TUTT; Sadler 1978). An interaction between the TUTT and a low-level vorticity maximum appears to occur for both cases resulting in a spinup of a tropical cyclone. Interestingly, this spinup process associated with upper- and lower-level disturbances is very similar to the process by which midlatitude and polar cyclones form (Shapiro et al. 1987; Whitaker et al. 1988; Businger 1991).

Potential vorticity has proven useful in understanding large-scale midlatitude dynamics, and its use is becoming more widely appreciated in tropical motion systems (Schubert and Hack 1983; Thorpe 1985; Schubert and Alworth 1987; Schubert et al. 1991). Previous work has confirmed the role of upper-level potential vorticity disturbances on the formation of midlatitude cyclones, fronts, and polar cyclones (Eliassen and Kleinschmidt 1957; Farrell 1982, 1984, 1985; Hoskins et al. 1985; Whitaker et al. 1988; Davis and Emanuel 1990; Thorncroft and Hoskins 1990; Montgomery 1990; Montgomery and Farrell 1990, 1991, 1992). In this work we investigate the influence of upper-level potential vorticity disturbances on tropical cyclone formation within the context of two simple

nonlinear balanced models that incorporate moist processes. Moist convection is modeled in a simple manner by assuming near neutrality in regions of forced ascent, but additional cooperative intensification mechanisms are neglected. In this model moist processes act to reduce the effective static stability to ascending parcels and provide a source/sink term in the evolution equation for dry potential vorticity.

Asymmetric interactions between upper- and low-level disturbances are first explored by studying the response of a balanced slab-symmetric vortex to upper-level momentum driving in a nearly moist neutral (but statically stable) tropical atmosphere. The second part investigates for the first time in a tropical context the fully three-dimensional balanced dynamics of such processes, and a conceptual model for tropical cyclone formation in association with upper-level potential vorticity forcing is proposed. We conclude by summarizing our results, and we point to future work, and discuss implications of the theory.

2. Symmetric response to external driving

In this section we adopt a simple balanced-vortex model for exploring the role of upper-level disturbances in tropical cyclone formation. All tilde variables will refer to dimensional variables, and nontilde variables will be dimensionless. Bold variables denote vector quantities. The flow model is a two-dimensional, slab-symmetric (i.e., $\partial/\partial\tilde{y} = 0$), Boussinesq geostrophic momentum model that approximates the horizontal momentum per unit mass vector by its geostrophic value, $\tilde{\mathbf{p}}_h \approx \tilde{\mathbf{v}}_g = (0, \tilde{v}_g)$ (Hoskins 1975). We assume geostrophic balance in the x direction. In the y direction an external force per unit mass, $\tilde{F}$, is applied to the fluid, inducing meridional accelerations, and an attendant secondary circulation in the x–z plane. Hydrostaticity and mass conservation for a Boussinesq fluid are assumed. The latent heat of condensation is represented by a heat source, $\tilde{\Theta}_S$, in the entropy equation for dry air, and as in previous work, ascending parcels are assumed saturated and to conserve saturated entropy. During parcel ascent all condensed water is assumed to rain out (or remain suspended in cloud), but on descent, parcels conserve dry entropy (Montgomery and Farrell 1991, hereafter referred to as MF).[1] Expressions for $\tilde{\Theta}_S$ and $\tilde{F}$ are given below.

The vortex model is given by

$$f\tilde{v}_g = \frac{\partial}{\partial\tilde{x}}\tilde{\phi}^{\text{total}} \tag{2.1a}$$

$$\left(\frac{\partial}{\partial\tilde{t}} + \tilde{u}_a\frac{\partial}{\partial\tilde{x}} + \tilde{w}\frac{\partial}{\partial\tilde{z}}\right)\tilde{v}_g + f\tilde{u}_a = \tilde{F}, \tag{2.1b}$$

$$\frac{g}{\tilde{\Theta}_0}\tilde{\Theta}^{\text{total}} = \frac{\partial\tilde{\phi}^{\text{total}}}{\partial\tilde{z}}, \tag{2.1c}$$

$$\left(\frac{\partial}{\partial\tilde{t}} + \tilde{u}_a\frac{\partial}{\partial\tilde{x}} + \tilde{w}\frac{\partial}{\partial\tilde{z}}\right)\tilde{\Theta}^{\text{total}} = \tilde{\Theta}_S, \tag{2.1d}$$

$$\frac{\partial\tilde{u}_a}{\partial\tilde{x}} + \frac{\partial\tilde{w}}{\partial\tilde{z}} = 0, \tag{2.1e}$$

where $\tilde{v}_g$ denotes the meridional geostrophic wind; $\tilde{\phi}^{\text{total}}$ denotes the total geopotential; $(\tilde{u}_a, \tilde{w})$ denote the zonal ageostrophic and vertical winds, respectively; $\tilde{\Theta}^{\text{total}}$ denotes the total potential temperature; $\tilde{\Theta}_0$ represents a characteristic surface temperature; and g and f denote the gravitational constant and the Coriolis parameter, respectively. The depth between the top of the boundary layer ($Z = 0.0$) and tropical tropopause is defined as H, and the tropopause is represented by an increased static stability below a rigid lid at $\tilde{Z} = H$. For simplicity, in this section we neglect Ekman pumping on $Z = 0$, so the boundary condition is that $\tilde{w}$ vanish on $\tilde{Z} = H$, 0. Zonal periodicity is also assumed.

The external force, $\tilde{F}$, is assumed to model an eddy momentum flux convergence at upper levels as in Challa and Pfeffer (1980), who illustrated the role of eddy momentum fluxes in hurricane development using Sundqvist's axisymmetric tropical cyclone model with cloud physics. Here, we associate the momentum flux convergence with upper-level migratory potential vorticity anomalies, and our goal is to understand vortex response with a simpler balanced model that incorporates moist processes. The current formulation extends the hurricane model of Gill (1982) by including finite Rossby number effects, and momentum driving.

In this work, the dry potential vorticity (henceforth referred to as PV) is adopted as a primary variable. Our definition for PV is

$$\tilde{Q}_g \equiv \frac{g}{f\tilde{\Theta}_0}\tilde{\boldsymbol{\omega}}_{\text{abs}}\cdot\nabla\tilde{\Theta}^{\text{total}},$$

and $\tilde{\boldsymbol{\omega}}_{\text{abs}}$ denotes the absolute vorticity evaluated with the geostrophic winds. We choose to define PV in units of the static stability since from a dynamical viewpoint it plays the same role as the dry static stability in the transformed dimensional system. In contrast to the quasigeostrophic system, however, the equivalent dry static stability is solution dependent and a function of space. An equivalent system [defined by (2.6) and (2.7)] is solved in terms of $\tilde{Q}_g$ in geostrophic coordinates

$$\tilde{X} = \tilde{x} + \frac{\tilde{v}_g}{f},$$

$$\tilde{Z} = \tilde{z},$$

$$\tilde{\Phi}^{\text{total}} = \tilde{\phi}^{\text{total}} + \frac{1}{2}\tilde{v}_g^2, \tag{2.2}$$

[1] In a recent paper on polar low dynamics, our interpretation of the moisture parameterization has been extended to include a moist unstable troposphere (Montgomery and Farrell 1992).

and transformed back to real coordinates. The heating term in the transformed system is given by

$$\tilde{\Theta}_S = \frac{\tilde{w}^* \tilde{Q}_g}{g}(1 - R(Z))H(\tilde{w})\tilde{\Theta}_0; \qquad (2.3)$$

$H(\tilde{w})$ denotes a Heaviside function such that $H = 1$ if $\tilde{w} > 0$ and $H = 0$ otherwise; $\tilde{w}^* = J^{-1}\tilde{w}$, where $J^{-1} = 1 - f^{-1}\partial \tilde{v}_g/\partial \tilde{X}$; and J denotes both the vertical component of the absolute vorticity and the Jacobian of the coordinate transformation. Finally, $R(Z)$ is a dimensionless stability parameter measuring the deviation from moist adiabatic ascent on absolute momentum surfaces fX = const. While we acknowledge that some form of air–sea interaction is needed to maintain a state of conditional neutrality, we neglect additional energy sources associated with CISK or air–sea interaction and their attendant intensification mechanisms. Of course, real convection also entrains, but for simplicity we neglect such complications in a first study in order to isolate the physics behind the upper-level forcing mechanism. The simulated balanced spinup should thus tend to underestimate the spinup that would occur if we included large-scale entrainment of midlevel air by the cumulus ensemble. Further details regarding the R parameter can be found in Montgomery and Farrell (1992) and references therein.

Scaling for (2.1) is as follows. Let N^2 denote the dry static stability, and F_0 represent a characteristic value of external forcing. For a characteristic horizontal length scale, we choose the Rossby deformation radius (NH/f), and for a characteristic vertical scale, we choose the height of the tropopause (H). For the time scale we choose (NH/F_0). Flow variables ($\tilde{\Phi}^{\text{total}}$, $\tilde{\Theta}^{\text{total}}$, $\tilde{v}_g$, $\tilde{w}$, $\tilde{Q}_g^{\text{total}}$) are scaled via

$$\tilde{\Phi}^{\text{total}} = N^2H^2[\Phi_h + \Phi] + gHZ$$

$$\tilde{\Theta}^{\text{total}} = \frac{\Theta_0}{g}\frac{\partial}{\partial \tilde{Z}}\tilde{\Phi}^{\text{total}} = \frac{\Theta_0 N^2 H}{g}[\Theta_h + \Theta] + \Theta_0$$

$$\tilde{v}_g = NHv_g = NH\frac{\partial \Phi}{\partial X}$$

$$\tilde{w} = \frac{F_0}{N}w$$

$$\tilde{u}_a = \frac{F_0}{f}u_a$$

$$\tilde{Q}_g^{\text{total}} = N^2Q_g = N^2(1 + q_g). \qquad (2.4)$$

In (2.4), Φ_h $(=Z^2/2)$ and Θ_h $(=Z)$ comprise the hydrostatic background state with uniform static stability; q_g is the anomalous dry potential vorticity; and Φ includes both the initial vortex structure and the increased static stability layer as a model for the tropical tropopause. Expressions for Φ are given below.

The external force is taken to be

$$\tilde{F}(X, Z) = -F_0 \sin\left(\frac{2\pi X}{L_X}\right)\sin\left[\frac{\pi}{D}(Z - Z_c)\right], \qquad (2.5)$$

for $Z_c \leq Z \leq Z_c + D$, and zero otherwise. The force is maximum at $Z = Z_c + D/2$, and D represents the depth of the upper-level forcing. The force (2.5) induces cyclonic flow at $X = L_X/2$ and anticyclonic flow at $X = 0$, where L_X represents the width of the computational domain. In this work, we choose $D = 0.4$ and $Z_c = 0.4$.

In this section, we choose $f = 5 \times 10^{-5}\ \text{s}^{-1}$, $N = 0.8 \times 10^{-2}\ \text{s}^{-1}$, $\tilde{\Theta}_0 = 300$ K, and a tropopause height of $H = 15$ km. Diagnostic analyses of hurricane intensity change in association with upper-level disturbances find momentum flux convergences of $\approx 26\ \text{m s}^{-1}\ \text{day}^{-1}$ (Molinari and Vollaro 1989). This implies $F_0 = 3 \times 10^{-4}\ \text{m s}^{-2}$. Hence, for these parameters, the horizontal length scale is 2400 km. The geostrophic velocity scale (NH) is 120 m s^{-1}, the vertical velocity scale (F_0/N) is 3.75 cm s^{-1}, and the zonal ageostrophic velocity scale (F_0/f) is 6 m s^{-1}. The potential-temperature scale $(\Theta_0 N^2 H/g)$ is 29.38 K, the potential vorticity scale (N^2) is $0.64 \times 10^{-4}\ \text{s}^{-2}$, and the time scale (NH/F_0) is 111 h.

In terms of anomalous dry potential vorticity, q_g, the dimensionless vortex equations are as follows:

$$\frac{D}{DT}q_g = H(w)J\frac{\partial}{\partial Z}[w^*(1 + q_g)(1 - R(Z))] + J\left[\left(1 + \frac{\partial \Theta}{\partial Z}\right)\frac{\partial F}{\partial X} - \frac{\partial \Theta}{\partial X}\frac{\partial F}{\partial Z}\right], \qquad (2.6a)$$

$$\frac{\partial}{\partial T}\Theta = 0, \quad \text{on} \quad Z = 0, 1 \qquad (2.6b)$$

$$(1 + q_g)\frac{\partial^2 \Phi}{\partial X^2} + \frac{\partial^2 \Phi}{\partial Z^2} = q_g, \qquad (2.6c)$$

$$\frac{\partial}{\partial X}\left[Q_{g_{\text{eff}}}\frac{\partial \psi}{\partial X}\right] + \frac{\partial^2}{\partial Z^2}\psi = \frac{\partial F}{\partial Z} + \frac{\partial (F, v_g)}{\partial (X, Z)}, \qquad (2.6d)$$

where

(A) $\dfrac{D}{DT} = \dfrac{\partial}{\partial T} + F\dfrac{\partial}{\partial X} + w\dfrac{\partial}{\partial Z}$

(B) $\dfrac{\partial (F, v_g)}{\partial (X, Z)} = \dfrac{\partial F}{\partial X}\dfrac{\partial v_g}{\partial Z} - \dfrac{\partial F}{\partial Z}\dfrac{\partial v_g}{\partial X}$

(C) $H(w)$ denotes the Heaviside function defined above.

(D) $Q_{g_{\text{eff}}} = \begin{cases} Q_g R(Z), & \text{when} \quad w > 0 \\ Q_g, & \text{when} \quad w \leq 0 \end{cases}$

(E) Deep saturated ascent in a nearly moist neutral tropical atmosphere is idealized by $R(Z) = R_0$, where R_0 is a small positive constant defined below.

(F)
$$w^* = -\frac{\partial \psi}{\partial X}$$
$$J^{-1} = 1 - \frac{\partial^2 \Phi}{\partial X^2}$$
$$w = Jw^*$$
$$u_a = +\frac{\partial \psi}{\partial Z} + w\frac{\partial v_g}{\partial Z}$$
$$Q_g = J\frac{\partial}{\partial Z}\theta^{\text{total}} = 1 + q_g. \qquad (2.7)$$

(G) Flow variables in physical coordinates (x, z) are obtained via the nonlinear transformation:

$$x = X - v_g(X, Z, T)$$
$$z = Z. \qquad (2.8)$$

Here X periodicity is assumed for all flow variables. Along the horizontal boundaries $Z = 1, 0$, we impose $\Theta = \partial\Phi/\partial Z$, and $\psi = 0$. Equations (2.6) comprise two prognostic equations for the interior potential vorticity (2.6a) and boundary potential temperature (2.6b), as well as two diagnostic equations expressing invertibility (2.6c) and thermal wind balance (2.3e). [The latter is analogous to the slab-symmetric version of Eliassen's streamfunction equation for the transverse circulation in a circular vortex under gradient wind balance (Eliassen 1951).] The numerical method for solving (2.6) is similar to previous work (MF), and the flow domain is a rectangle whose X and Z dimensions are L_X and 1, respectively. The elliptic equations (2.6c) and (2.6d) are solved by SOR on a uniform rectangular grid with 33^2 points. The nondimensional time step increment used is 1/72 and corresponds dimensionally to 1.54 h. The applied forcing is held constant in time and produces both positive and negative PV anomalies. Integrations are terminated when the total PV, $1 + q_g$, becomes negative.

Up to this point we have treated $R(Z)$ as a "free parameter," but in reality, low-level tropical disturbances, such as easterly waves or tropical cloud clusters, play a dual role by providing an initial vorticity disturbance and helping establish a near-moist neutral environment. Thus, although our model formulation formally treats R and the initial flow as independent parameters, we henceforth assume that the initial low-level disturbance has already established a moist neutral state. A nearly moist neutral atmosphere is represented by choosing a small value of R_0 in (D). In this section, we use $R_0 = 0.01$ for moist dynamics and $R_0 = 1$ for dry dynamics.

Also note that the magnitude of the external force, F_0, has purposely been scaled out of the dynamics (2.6)–(2.8), and only enters the interpretation of the results via the ageostrophic winds and the time scale.

a. Examples

The physics of spinup is illustrated with the initial condition

$$\Phi = \frac{1}{5}Z^6 + A\cos(kX)\exp(-\gamma Z), \qquad (2.9)$$

where $A = 1/50$, $\gamma = 2.3$, and $k = 5$. The initial flow is a superposition of a quiescent tropopause layer and a cyclonic surface vortex centered at $X = 0.63$. The upper-level forcing, F, and the y velocity, v_g, associated with (2.9) both vary as $-\sin(kX)$. The results for the moist case are summarized in Figs. 1a–1c, and salient features are discussed below.

1) Geostrophic wind and Anomolous PV

Figure 1a displays the meridional geostrophic velocity, v_g, and the anomalous PV, q_q, at $T = 0.0$, 0.25, and 0.61 nondimensional times (0, 27.7, and 67.7 h). Note the changing contour interval for both plots. Initially, the maximum geostrophic wind is at the surface (12 m s^{-1}) with a diameter of maximum winds of approximately 1500 km. By $T = 0.61$, the upper-level forcing has created a strong PV maximum at upper levels along with a thin tube of PV that extends down to the surface. A secondary maximum is evident on $Z = 0$. In association with the primary PV maximum, the winds are greatest at upper levels. The induced low-level potential vorticity, however, coincides with an increased surface wind and a substantial scale contraction of the surface vortex. The surface winds increase from 0.1 (12 m s^{-1}) to 0.18 (21.6 m s^{-1} during this time.

2) Absolute vorticity

Figure 1b shows the vertical component of the absolute vorticity normalized by f for the same times of Fig. 1a. Since the vertical component of the absolute vorticity and Jacobian are proportional to one another, we will refer to them interchangeably. The maximum absolute vorticity is initially $2f$ on the surface. At $T = 0.61$ the absolute vorticity has increased rapidly to $25f$. Near $X = 0.63$, the applied force produces cyclonic vorticity at upper levels, but the dominant vorticity increase occurs on the surface. Note also that the scale of the surface vorticity shrinks dramatically during this time.

3) Vertical velocity and potential temperature

Figure 1c displays the potential-temperature anomaly Θ (which includes the model tropopause layer) and the vertical velocity w for the same times of Fig. 1a. At $T = 0.0$, (2.9) gives a warm surface anomaly centered at $X = 0.63$, but the anomaly is not indicated due to the large contour interval used.

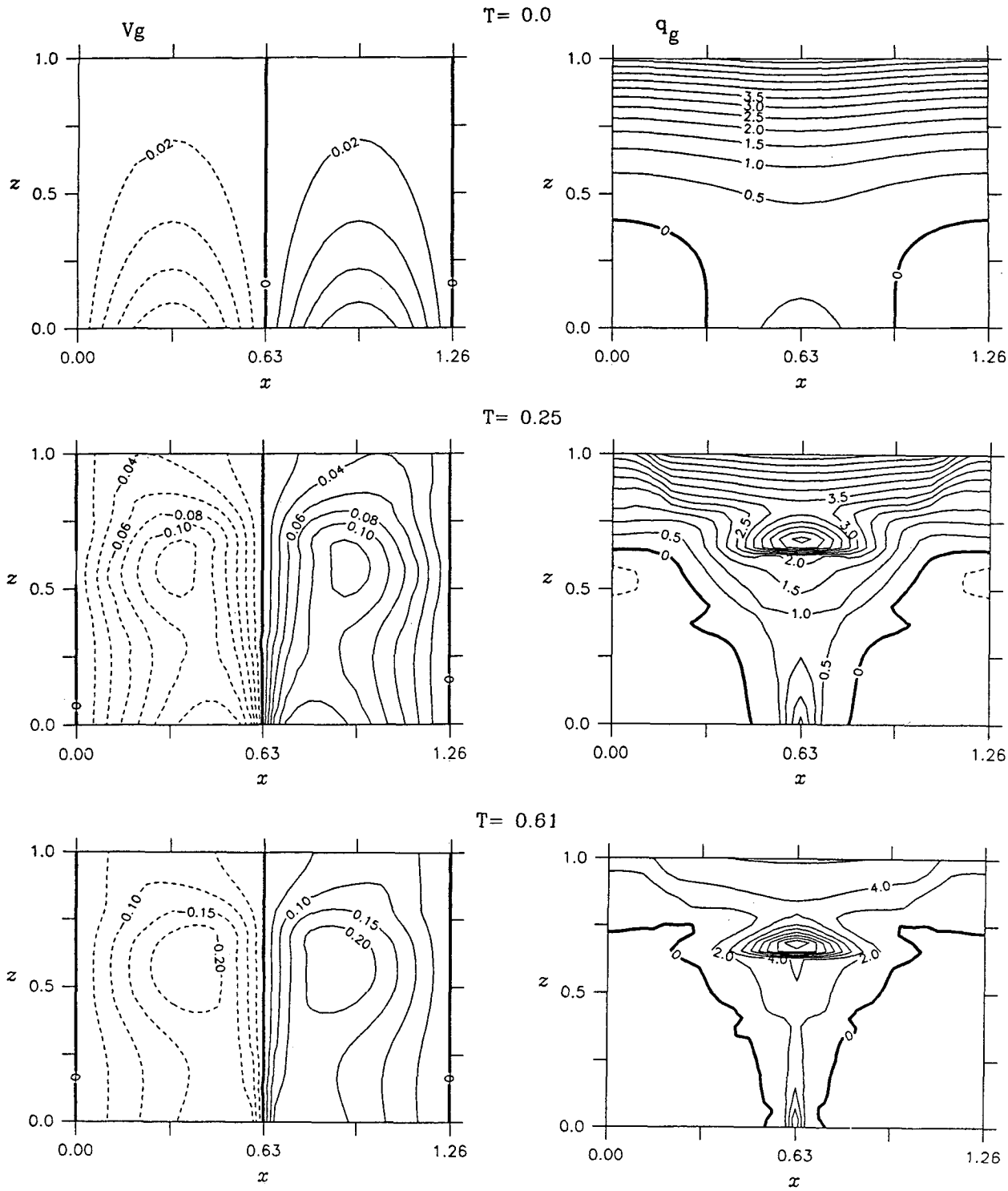

FIG. 1a. Moist 2D vortex dynamics ($R = 0.01$) subject to upper-level momentum driving for the initial condition (2.9) at $T = 0.0$, 0.25, and 0.61 nondimensional times (0.0, 28, and 68 h, respectively). The left column displays contour plots of the the meridional velocity, v_g, while the right column displays the anomalous PV, $q_g \equiv Q_g - 1$. At $T = 0.0$, the contour intervals for v_g and q_g are 0.02 and 0.50, respectively, though they subsequently change with time. Solid lines denote positive values, dashed lines denote negative values, and bold lines denote the zero contour. Unit values of v_g and q_g correspond to 120 m s^{-1} and 0.64×10^{-4} s^{-2}, respectively.

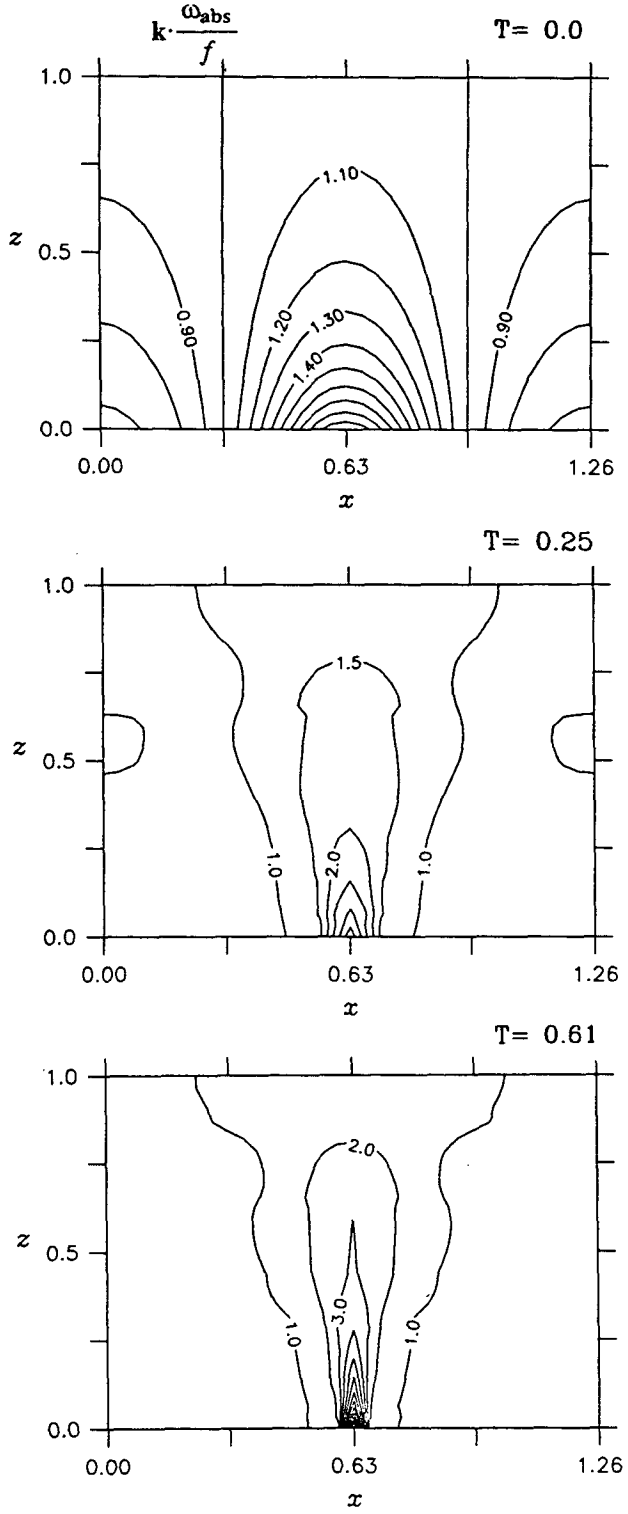

FIG. 1b. Moist 2D vortex dynamics (R = 0.01) as in Fig. 1a. Shown are contour plots of the vertical component of the absolute vorticity normalized by f, $\mathbf{k} \cdot \boldsymbol{\omega}_{abs}/f$. Note the changing contour interval. Solid lines denote positive values. A unit value corresponds to an absolute vorticity of $1/f$.

Now, in order to satisfy thermal-wind balance, the intensifying upper cyclone requires descending motion to heat the column above it and ascending motion to cool the column below it. For a nearly moist neutral atmosphere, the small static stability in ascent regions prevents a substantial change in thermal structure despite large vertical velocities. The Θ plot at $T = 0.61$ exhibits a small cooling in the core of the upper cyclone. Thus, to preserve thermal-wind balance, stronger ascending motions are generally required. A substantial asymmetry with respect to the strength of ascending and descending motions is evident in both w plots. Upward velocities increase slightly from 0.53 at $T = 0.0$ to 0.56 at $T = 0.61$, and the width of the ascent region shrinks during this period.

The assumption of deep moist neutrality has important implications for vorticity dynamics: As $R \to 0$, ascending regions extend much farther down into the lower troposphere than would occur in a dry atmosphere (i.e., for $R = 1$). Therefore, for moist dynamics, we expect significantly stronger low-level vortex stretching and consequently enhanced coupling between upper- and lower-level disturbances.

Results for dry dynamics ($R \equiv 1.0$) using the same initial condition are displayed in Figs. 2a and 2b. Figure 2a shows the meridional velocity v_g, the anomalous PV q_g, and the absolute vorticity at $T = 0.5$. In this case, upper-level forcing produces a more localized upper cyclone and a very weak spinup at low levels. Figure 2b shows Θ and w at $T = 0.0$ and 0.5. Rising motion is confined to upper levels and is only half as strong as in the case of moist neutral dynamics.

Thus, for dry dynamics, upper-level forcing produces an upper cyclone with minimal surface development. For nearly moist neutral dynamics, upper-level forcing promotes surface development through deep ascending motions required to maintain thermal-wind balance. Moist development is accompanied by a rapid scale contraction to subsynoptic scales. These conclusions are in accord with those of Shi et al. (1990, see their Fig. 11), who, in part of their study, employed a primitive equation model to study the atmospheric response to upper-level momentum driving with and without cumulus convection.

3. Three-dimensional PV dynamics

In the previous section, the symmetric response to upper-level driving was studied as an idealization of asymmetric interactions between upper- and lower-level PV disturbances. Here, we investigate the fully three-dimensional balanced PV dynamics of such processes in a nearly moist neutral tropical atmosphere. We employ the geostrophic momentum approximation with moist processes modeled as in section 2. The model is based on the three-dimensional Boussinesq geostrophic momentum model (abbreviated hereafter as GM) developed by Hoskins (1975), Hoskins and Draghici (1977), and Heckley and Hoskins (1982).

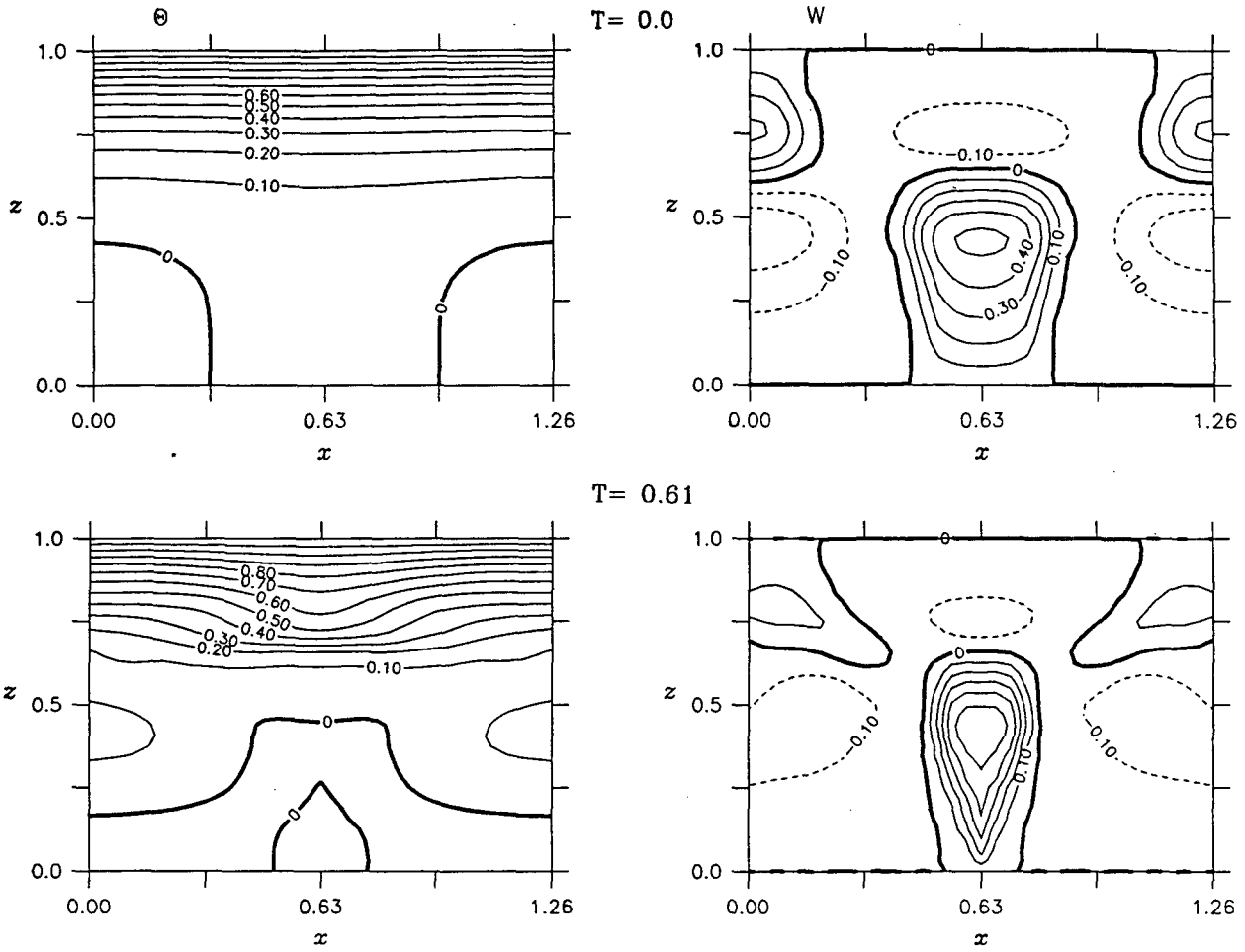

FIG. 1c. Moist 2D vortex dynamics ($R = 0.01$) as in Fig. 1a at $T = 0.0$ and 0.61 (0.0 h and 68 h, respectively). The left column displays contour plots of the potential temperature anomaly Θ, while the right column displays the vertical velocity w. Solid lines denote positive values, dashed lines denote negative values, and bold lines denote the zero contour. Unit values of Θ and w correspond to 29.4 K and 3.75 cm s^{-1}, respectively.

The model is integrated in geostrophic coordinates (X, Y, Z) given by (3.5e)–(3.5g). We further assume that the combination of moist convection and moist enthalpy sea-to-air fluxes merely maintain a state of moist neutrality to ascending parcels. Additional energy sources associated with CISK or air–sea interaction are neglected, and the planetary boundary layer is parameterized with an Ekman layer (described below).

The consistency of the three-dimensional GM approximation has been established for certain uniform potential vorticity flows (Hoskins 1976). More recently, however, Snyder et al. (1991) have found systematic differences between the primitive equations and the geostrophic momentum equations with respect to the horizontal phase tilt of baroclinic waves and the strengths of the model anticyclones. Nevertheless, their study shows relatively small discrepancies between the strengths of the model cyclones. Thus, despite these differences in detail, the GM model appears to contain the basic elements for describing the cyclogenesis process. We believe that a basic understanding of tropical cyclone formation, and perhaps even certain aspects of tropical cyclone development, can be obtained with this relatively simple three-dimensional balanced system.

a. 3D model formulation

Notational conventions are the same as in section 2. Nomenclature for the basic-state and disturbance flow configurations can be briefly described in terms of the modified geopotential $\tilde{\Phi} = \phi + \frac{1}{2}(\tilde{u}_g^2 + \tilde{v}_g^2)$. The hydrostatic state for a troposphere with uniform static stability is denoted as $\tilde{\Phi}_h$. The tropical tropopause is represented by an increased static stability below a rigid upper lid at $\tilde{Z} = H$; the tropopause part is denoted by $\tilde{\Phi}_{tr}$. The static stability increases monotonically with the most rapid increase near the upper lid. The

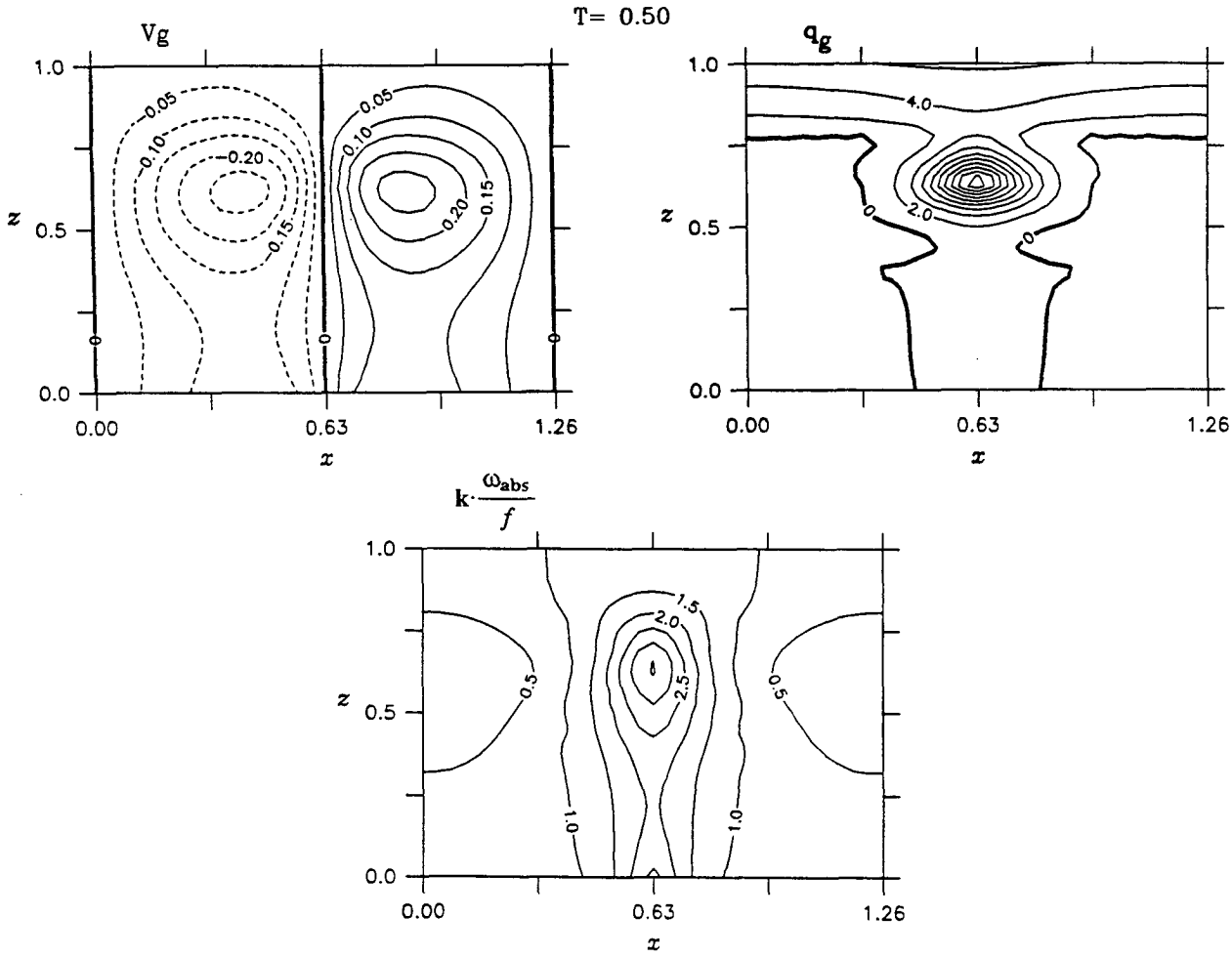

FIG. 2a. Dry 2D vortex dynamics (R = 1.0) subject to upper-level momentum driving for the initial condition (2.9) at T = 0.5 (55.5 h). Shown are the meridional geostrophic wind, v_g, the anomalous PV, q_g, and the absolute vorticity divided by f. Solid lines denote positive values, dashed lines denote negative values, and bold lines denote the zero contour. Unit values of v_g, q_g, and normalized absolute vorticity are the same as in Fig. 1a.

finite-amplitude flow structures that comprise the upper- and lower-level disturbances will be denoted, respectively, by $\tilde{\Phi}'_u$ and $\tilde{\Phi}'_l$; their sum will be denoted by $\tilde{\Phi}'$.

An illustrative example is the case of tropical storm Diana (Bosart and Bartlo 1991; Reilly and Emanuel 1991). Diana formed in the subtropics in September 1984 in conjunction with a westerly moving upper-level PV anomaly and a surface front off the northeastern coast of Florida. The observed basic-state flow consisted of a weak westerly flow at upper levels ($\tilde{Z}$ = H), no motion on Z = 0, and a weak surface temperature gradient. For simplicity, we choose

$$\bar{\tilde{U}}(\tilde{Z}) = U_0\left(\frac{\tilde{Z}}{H}\right)^2, \qquad (3.1)$$

where U_0 is a characteristic velocity magnitude defined below. Relative motion between upper-level troughs and low-level disturbances does not occur without some vertical shear of the horizontal winds. Thus, (3.1) may be widely applicable to other tropical flows possessing upper-level westerlies and low-level easterlies, perhaps under a suitable Galilean transformation. In terms of the modified geopotential the corresponding basic-state flow [defined in (3.3)] is denoted as $\bar{\tilde{\Phi}}$ and we choose U_0 = 17 m s^{-1}.

Parameters for the three-dimensional model are chosen to be consistent with the Diana case, but the results are believed representative of many subtropical developments. The choice of scaling and a list of nondimensional parameters are given in Table 1. The horizontal scale is 1333 km and corresponds to the ambient Rossby deformation radius. The vertical scale is 12 km and represents the approximate depth between the subtropical tropopause and the top of the boundary layer. One advective time unit corresponds to 21.78 h, the horizontal velocity scale is 17 m s^{-1}, the vertical

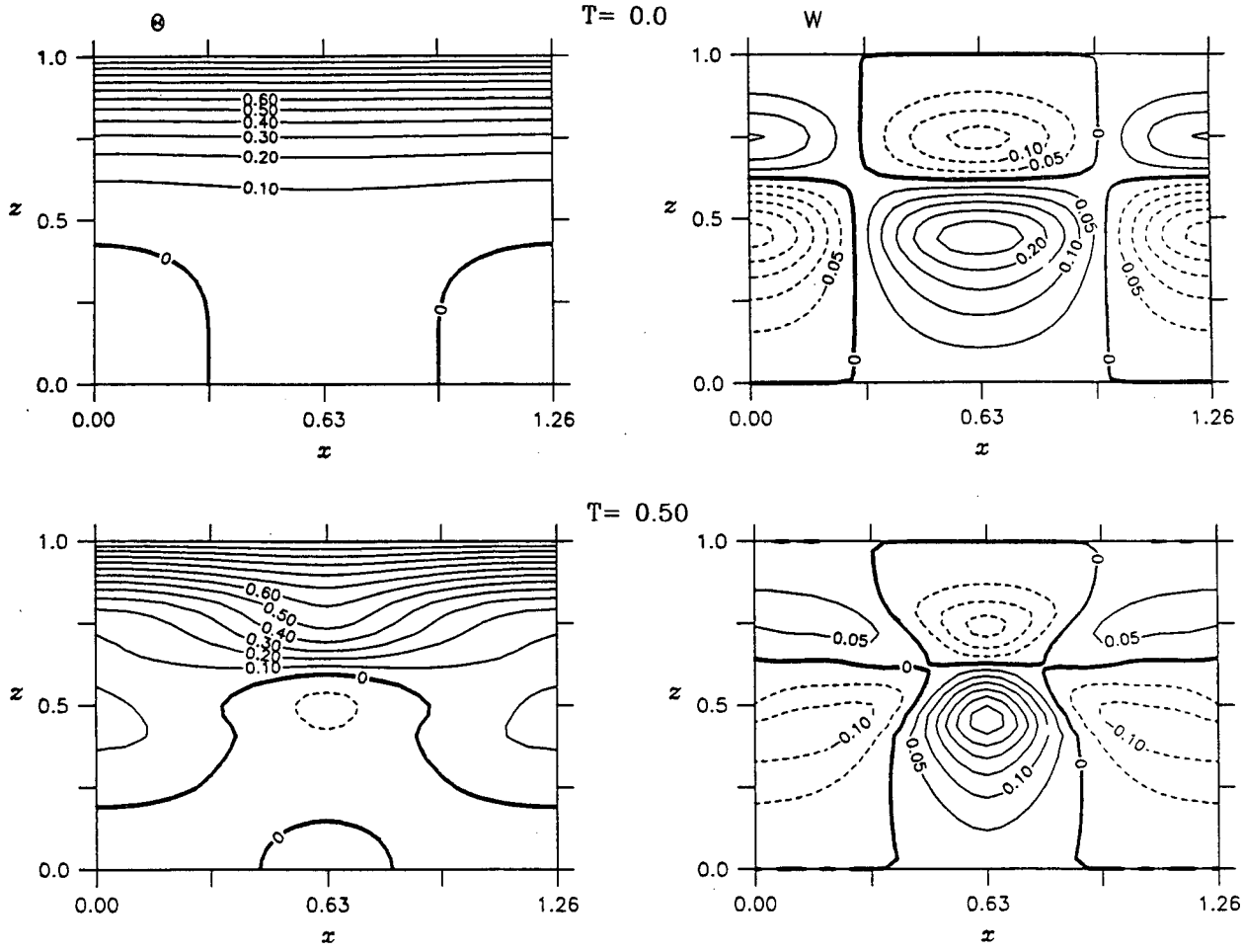

FIG. 2b. Dry 2D vortex dynamics (R = 1.0) as in Fig. 2a at T = 0.0, and 0.5 (0.0, 55.5 h, respectively). The left column displays contour plots of the potential temperature anomaly, Θ, while the right column displays the vertical velocity, w. Plotting conventions and characteristic values for Θ and w are the same as in Fig. 1c.

velocity scale is 15.3 cm s^{-1}, and the temperature scale is 23 K. If we assume a boundary-layer depth of approximately 1 km, then $\tilde{Z}$ = 1.0 corresponds to 13 km. The ambient zonal wind at $\tilde{Z}$ = 0.75 (≈10 km) is 9.56 m s^{-1}, while the zonal wind at $\tilde{Z}$ = 0.5 (≈7 km) is 4.25 m s^{-1}. Scaled expressions for the total fields ($\tilde{\Phi}^{\text{total}}$, $\tilde{\Theta}^{\text{total}}$, $\tilde{\mathbf{u}}_g^{\text{total}}$, $\tilde{w}$, $\tilde{Q}_g^{\text{total}}$) are

$$\tilde{\Phi}^{\text{total}} = N^2H^2\left[\Phi_h + \Phi_{tr} + \frac{1}{\sqrt{R_i}}(\bar{\Phi} + \Phi')\right] + gHZ$$

$$\tilde{\Theta}^{\text{total}} = \frac{\Theta_0}{g}\frac{\partial}{\partial \tilde{Z}}\tilde{\Phi}^{\text{total}} = \frac{\Theta_0 N^2 H}{g}\left[\Theta_h + \Theta_{tr} + \frac{1}{\sqrt{R_i}}(\bar{\Theta} + \Theta')\right] + \Theta_0$$

$$\tilde{\mathbf{u}}_g^{\text{total}} = \frac{\mathbf{k}}{f} \times \tilde{\nabla}_H \tilde{\Phi}^{\text{total}} = U_0\,\mathbf{u}_g$$

$$\tilde{w} = f\frac{U_0}{N}w$$

$$\tilde{Q}_g^{\text{total}} = N^2 Q_g \tag{3.2}$$

and

$$\Phi_h = \frac{Z^2}{2}, \quad \Theta_h = Z$$

$$\Phi_{tr} = \frac{1}{5}Z^6, \quad \Theta_{tr} = \frac{6}{5}Z^5$$

$$\bar{\Phi} = -\left(Y - \frac{L_Y}{2}\right)Z^2$$

$$\bar{\Theta} = -2\left(Y - \frac{L_Y}{2}\right)Z, \tag{3.3}$$

where L_Y denotes the meridional width of the computational domain. Expressions for Q_g and Φ' are given

TABLE 1. Parameters for the three-dimensional geostrophic momentum system defined in section 3. See MF, and Montgomery and Farrell (1992), for further details concerning the R parameter, and text for values used.

Model parameters

$$N^2 = 0.64 \times 10^{-4}\ \mathrm{s}^{-2}$$

$$H = 12\ \mathrm{km}$$

$$f = 0.72 \times 10^{-4}\ \mathrm{s}^{-1}$$

$$U_0 = 17\ \mathrm{m\ s}^{-1}$$

$$L_R = \frac{NH}{f} = 1333\ \mathrm{km}$$

$$T = L_R U_0^{-1} = \sqrt{R_i} f^{-1} = 21.78\ \mathrm{h}$$

$$C_D = 2 \times 10^{-3}$$

Dimensionless parameters

$$\mathrm{R_i} = \frac{N^2 H^2}{U_0^2} = 31.88$$

$$\delta = \frac{C_D U_0}{fH} = 3.93 \times 10^{-2}$$

$$R = \frac{\Gamma_m Q_{ge}}{\Gamma_d Q_g}$$

below, and $R_i = N^2H^2/U_0^2$ is a characteristic Richardson number of the basic-state flow.

In terms of the total dry potential vorticity Q_g, the nondimensional moist GM equations are

$$\left(D_g + w\frac{\partial}{\partial Z}\right)Q_g = H(w)J\frac{\partial}{\partial Z}\left[w^*Q_g(1 - R(Z))\right], \tag{3.4a}$$

$$D_g\Theta = 0, \quad \text{on} \quad Z = 1 \tag{3.4b}$$

$$D_g\Theta + \sqrt{R_i}w^*Q_g = \sqrt{R_i}H(w^*)w^*Q_g(1 - R(Z)), \quad \text{on} \quad Z = 0 \tag{3.4c}$$

$$Q_g\nabla_H^2\Phi' + \frac{\partial^2\Phi'}{\partial Z^2} = \sqrt{R_i}(Q_g - 1) - \frac{\partial^2}{\partial Z^2}(\sqrt{R_i}\Phi_{tr} + \bar{\Phi}) + \frac{Q_g}{\sqrt{R_i}}\left(\frac{\partial^2\Phi'}{\partial X^2}\frac{\partial^2\Phi'}{\partial Y^2} - \frac{\partial^2\Phi'}{\partial X\partial Y}\right),$$

$$\nabla_H^2[Q_{g_{eff}}w^*] + \frac{\partial^2}{\partial Z^2}w^* = \frac{-2}{\sqrt{R_i}}\nabla_H\cdot\mathbf{F} - \frac{1}{R_i}\frac{\partial}{\partial Z}D_g\frac{\partial(u_g, v_g)}{\partial(X, Y)}, \tag{3.4d,e}$$

where

(A) $\nabla_H = \left(\dfrac{\partial}{\partial X}, \dfrac{\partial}{\partial Y}\right)$

(B) $\dfrac{\partial(u_g, v_g)}{\partial(X, Y)} = \dfrac{\partial u_g}{\partial X}\dfrac{\partial v_g}{\partial Y} - \dfrac{\partial u_g}{\partial Y}\dfrac{\partial v_g}{\partial X}$

(C) $D_g = \dfrac{\partial}{\partial T} + \mathbf{u}_g\cdot\nabla_H$

(D) $\Theta = \bar{\Theta} + \Theta'$

(E) $\mathbf{F} = \left[\left(\dfrac{\partial\mathbf{u}_g}{\partial X}\right)\cdot\nabla_H\Theta, \left(\dfrac{\partial\mathbf{u}_g}{\partial Y}\right)\cdot\nabla_H\Theta\right]$

(F) $H(w)$ is the Heaviside function defined in section 2

(G) $Q_{g_{eff}} = \begin{cases} Q_g R(Z), & \text{when} \quad w > 0 \\ Q_g, & \text{when} \quad w \leq 0 \end{cases}$ (3.5a)

(H) The moist stability parameter $R(Z)$ is defined below.

(I)

$$w = Jw^*$$

$$J^{-1} = 1 - \frac{1}{\sqrt{R_i}}\nabla_H^2\Phi' + \frac{1}{R_i}\left(\frac{\partial^2\Phi'}{\partial X^2}\frac{\partial^2\Phi'}{\partial Y^2} - \frac{\partial^2\Phi'}{\partial X\partial Y}\right)$$

$$Q_g = J\frac{\partial}{\partial Z}\Theta^{\text{total}} \tag{3.5b,c,d}$$

(J) The fields in physical coordinates (x, y, z) are obtained via

$$x = X - \frac{1}{\sqrt{R_i}}v_g(X, Y, Z, T)$$

$$y = Y + \frac{1}{\sqrt{R_i}}u_g(X, Y, Z, T)$$

$$z = Z. \tag{3.5e,f,g}$$

Boundary conditions on the geopotential Φ' are that it remain doubly periodic in X and Y and satisfy $\Theta' = \partial\Phi'/\partial Z$ along the horizontal boundaries $Z = 0, 1$. Boundary conditions on the vertical velocity are that w (hence w^*) remain doubly periodic in X and Y; $w = 0$ on $Z = 1$; and $w = Jw^* = \delta\mathbf{k}\cdot\nabla_r\times\boldsymbol{\tau}^{(s)}$ on $Z = 0$. In the latter, the dimensionless parameter $\delta = C_DU_0/fH$, ∇_r denotes the gradient operator in real coordinates,[2] and $\boldsymbol{\tau}^{(s)}$ is the nondimensional horizontal surface stress vector. A simplified form of the quadratic stress relationship described in Gill [1982; see Eq. (9.5.1)] is used:

$$\boldsymbol{\tau}^{(s)} = |\mathbf{u}_g|\mathbf{u}_g(X, Y, 0, T). \tag{3.5h}$$

Using a drag coefficient of $C_D = 2 \times 10^{-3}$, the parameter values in Table 1 give $\delta = 3.93 \times 10^{-2}$. Further details concerning the numerical method and boundary conditions are discussed in the Appendix.

The basic format of (3.4) is the same as (2.6), except that we solve the three-dimensional omega equation

[2] See Appendix of Montgomery and Farrell (1992) for explicit formulas for ∇r in geostrophic coordinates.

(3.4e) instead of two streamfunction equations for the secondary circulation. The computational domain is a rectangular cube whose X, Y, and Z dimensions are L_X, L_Y, and 1, respectively. We have chosen $L_X = 5$ and $L_Y = 3.5$, corresponding to a horizontal domain of 6665 km × 4665 km. Let L, M, and N denote the number of panels in the X, Y, and Z directions, respectively. The horizontal grid increments in geostrophic space are then $\delta X = L_X/L$ and $\delta Y = L_Y/M$, whereas the vertical grid increment is $\delta Z = 1/N$. With $L = M = 32$, and $N = 16$, this corresponds to a horizontal grid resolution in geostrophic coordinates of 208 km in X, 145 km in Y, and a vertical resolution of 750 m. The nondimensional time step increment used in this section is 1/36, and corresponds dimensionally to 36.3 minutes. Recall that the transformation from geostrophic coordinates to real coordinates compresses regions where J is greater than unity and stretches regions where J is less than unity so that regions of high vorticity are well resolved and the coordinate transformation often more than doubles the resolution in these regions. For completeness, a few examples were run at a higher spatial and temporal resolution corresponding to $L = 48$, $M = 36$, $N = 16$, and $DT = 1/72$. The simulated cyclones were slightly stronger, but the principle flow features (discussed below) remained unchanged. Therefore, we believe the chosen resolution is sufficient for illustrating the basic physics.

As stated in section 2, we assume that low-level disturbances have already established a moist neutral environment. For moist dynamics two simple models for the moist stability parameter $R(Z)$ are considered. Moderately deep saturated ascent with a rapid adjustment to a strongly stable layer near the tropopause is modeled by $R(Z) = R_0 + (1 - R_0)Z^6$, and R_0 measures the deviation from moist neutrality. Deep saturated ascent in a moist neutral environment is modeled by $R(Z) = R_0$. For moist dynamics, we use $R_0 = 0.03$, and we use $R \equiv 1.0$ for dry dynamics.

b. 3D model results

Initial conditions prior to the formation of Diana comprise a meridionally elongated upper-level PV anomaly upwind of a surface front. The formation of such PV structures is not uncommon in extratropical flows [e.g., Fig. 10.4 in Palmen and Newton (1969) or Figs. 7e and 7f in Thorncroft and Hoskins (1990)]. This particular disturbance came from an extratropical synoptic-scale trough that underwent strong deformation (Bosart and Bartlo 1991). For simplicity, the surface front is idealized as a radially symmetric positive PV anomaly possessing a cold temperature perturbation at low levels. Letting u and l denote the upper and lower disturbances, respectively, expressions for these disturbances in geostrophic space are

$$\Phi'_u = \frac{A_u}{1 + 3(\delta X^2 + \frac{1}{3}\delta Y^2)} \frac{1}{1 + 4(Z - Z_u)^2},$$

$$\Phi'_l = \frac{A_l}{1 + 1.5R_l^2} \frac{1}{1 + 8(Z - Z_l)^2}, \tag{3.6a}$$

where

$$\delta X^2 = (X - X_u)^2, \quad \delta Y^2 = (Y - Y_u)^2$$
$$R_l^2 = (X - X_l)^2 + (Y - Y_l)^2$$
$$A_u = -\frac{25}{40}, \quad A_l = -\frac{20}{40}. \tag{3.6b}$$

The upper disturbance is centered at $(X_u, Y_u, Z_u) = (1.7, 1.75, 0.7)$, and the lower disturbance is centered at $(X_l, Y_l, Z_l) = (2.5, 1.75, 0.2)$. East is defined as positive X, and north is defined as positive Y. The relative vorticity of the upper disturbance is approximately $1.5f$, while the lower disturbance has a relative vorticity maximum at $Z = 0.2$ of approximately $0.5f$. These values are consistent with the analyses of Bosart and Bartlo at 1200 UTC 7 September 1984 prior to the cyclone formation phase.

Example 1. For the first example, we assume moderately deep saturated ascent. Good development is found in this case. Results are shown in Figs. 3a–d, and salient features are discussed.

1) POTENTIAL VORTICITY AND VERTICAL VELOCITY

Figure 3a shows three snapshots of the total potential vorticity field Q_g at $T = 0$, 2, and 4 advective times corresponding to 0, 43, and 86 h, respectively. Contour plots of horizontal sections of Q_g are shown in the left column of Fig. 3a, while the right column shows meridional cross sections (Y = const). Meridional sections are taken through the absolute vorticity maximum on $Z = 0$. Figure 3b shows the vertical velocity at $T = 4.0$ in the same format as Fig. 3a. A horizontal cross section of w on $Z = 0.25$ is included in the bottom center. Note the changing contour interval for w.

Initially, the upper PV anomaly is slightly underneath the tropopause layer and has an initial horizontal scale of approximately 600 km. The upper-level anomaly induces ascending motion in front of it and descending motion behind it. The maximum vertical velocity occurs at approximately $Z = 0.5$, with a secondary maximum in front of the low-level PV anomaly. The asymmetry between ascending and descending motion and the deep narrow region of rising air (noted in section 2) is evident.

By $T = 4$ (86 h), a small-scale PV maximum has formed near $(x, y) = (3.0, 2.4)$, with a dimensionless maximum of 3.4. Latent heat release within the deep ascent region (see Fig. 3b) produces a narrow "tube" of PV that extends from $Z = 0$ to upper levels. The PV maximum near $Z = 0.7$ is associated with the initial upper-level PV anomaly that is advected around the developing low-level PV anomaly; at $T = 2$ the upper anomaly lies slightly south of the meridional section

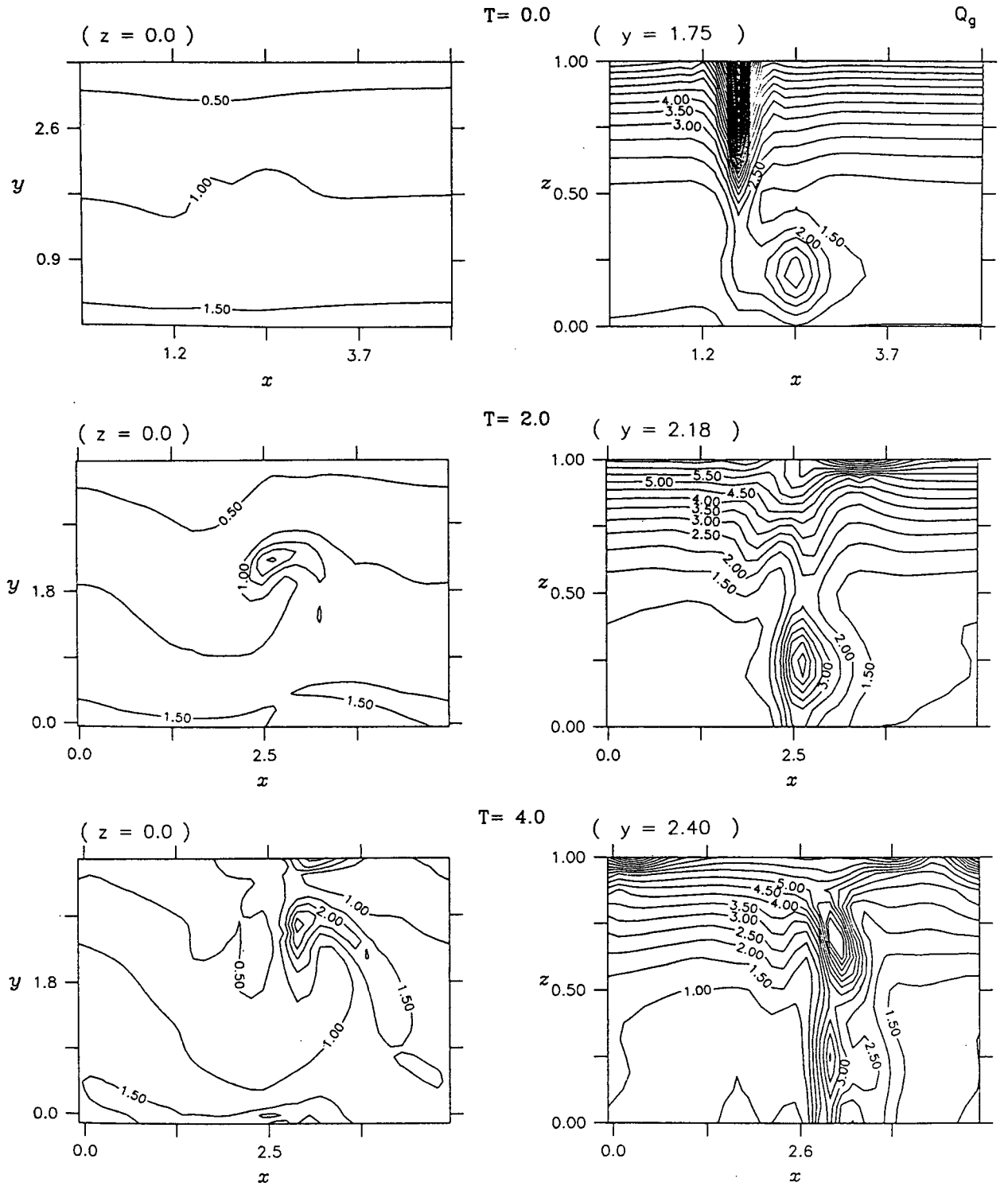

FIG. 3a. Moist 3D dynamics for example 1, assuming moderately deep neutrality ($R = R_0 + (1 - R_0)Z^6$, $R_0 = 0.03$) at $T = 0.0$, 2.0, and 4.0 (0.0, 43.5, and 87 h, respectively). The initial condition is given by (3.6). Shown are contour plots of the nondimensional total PV, (Q_g), at the top of the boundary layer $Z = 0.0$ ($\approx$1 km), and through a meridional cross section corresponding to the maximum absolute vorticity on $Z = 0.0$. The contour interval is fixed at 0.50. Solid lines denote positive values, and one horizontal unit of distance corresponds to 1333 km. The dimensional PV is obtained via $\tilde{Q}_g = N^2 Q_g$.

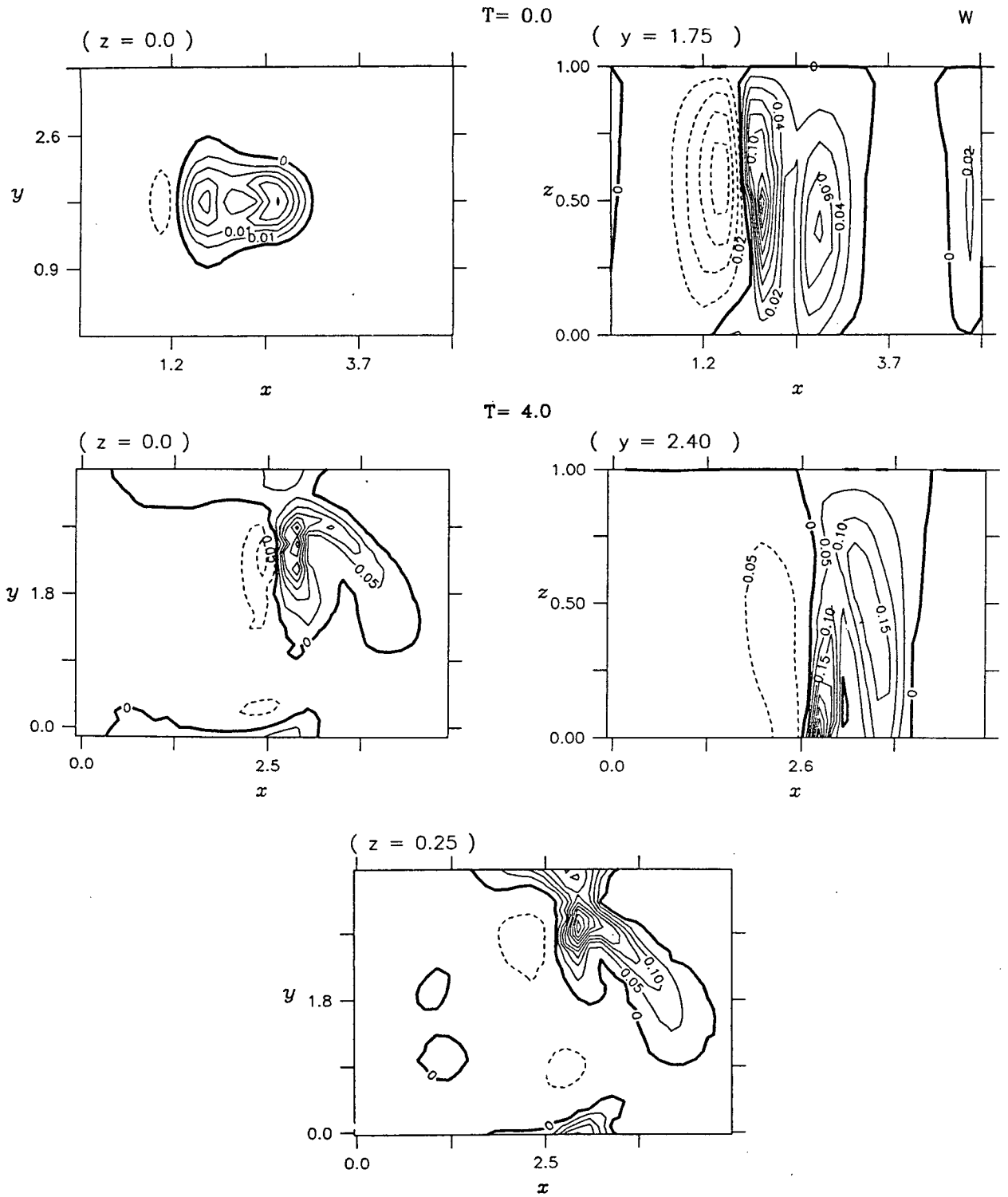

FIG. 3b. Moist 3D dynamics for example 1 (as in Fig. 3a) at $T = 0.0$, 2.0, and 4.0 (0 h, 43.5 h, and 87 h, respectively). Shown on the left are contour plots of the nondimensional vertical velocity w at the top of the boundary layer $Z = 0.0$. On the right are meridional cross sections of w. At the bottom center is a contour plot of w on $Z = 0.25$ ($\approx$4 km) at $T = 4.0$. Note the changing contour interval. A unit value of w corresponds to 15.3 cm s^{-1}. Solid lines denote positive values, dashed lines denote negative values, and bold lines denote the zero contour.

and hence is not evident (cf. Fig. 4b). On $Z = 1.0$, diabatic processes reduce the dimensionless potential vorticity to a minimum of 4.34 (relative to an ambient value of approximately 7) in the ascent region (not shown). The uppermost portion of the initial PV anomaly has moved northeastward over the surface PV maximum (not shown). At $T = 4.0$, maximum ascent occurs at approximately $Z = 0.25$ with an upward velocity of 0.49, or 7.49 cm s^{-1}. At the top of the boundary layer, the upward velocity has a maximum of 0.44, or 6.73 cm s^{-1}, and coincides with the induced PV maximum.

Also by $T = 4.0$, the surface PV maximum is nearly surrounded by air rising out of the boundary layer, and the meridional cross section of the vertical velocity shows two ascending currents rising out of the boundary layer. Note the beginning of a spiral PV structure on $Z = 0.0$. At $Z = 0.25$ the region of upward motion acquires a more north–south orientation but still tends to surround the developing storm. The asymmetric spiral pattern of rising moist air is consistent with satellite images showing comma cloud shapes that partially encircle Diana, as well as for many developing tropical cyclones (Frank 1987). The small tube of ascending air at upper levels is qualitatively similar to the analyzed vertical motion field within tropical storm Diana (Bosart and Bartlo 1991).

2) ABSOLUTE VORTICITY

Figure 3c shows the vertical component of the absolute vorticity normalized by f(Jacobian) at $T = 0.0$, 2.0, and 4.0 in the same format as Fig. 3a. At $T = 0.0$ the vertical structure of the absolute vorticity field tilts slightly westward with height and represents a favorable configuration for development in an upper-level westerly shear. At $T = 2.0$ the maximum absolute vorticity occurs at $Z = 0.3$ with a maximum of $2.5f$, and at $T = 4.0$ the maximum absolute vorticity is found on $Z = 0.0$ with a value of $3.16f$. The spinup sequence consists of a midlevel spinup followed by spinup at low levels. Observations of the transformation from a tropical disturbance into a tropical depression report a similar vorticity spinup sequence (Yanai 1968; see Figs. 10 and 11). Note also the scale contraction in the PV and absolute vorticity fields.

3) HEIGHT FIELD AND HORIZONTAL WINDS

Vector plots of the nondimensional geostrophic winds $\mathbf{u}_g$ in geostrophic coordinates are shown in Fig. 3d at $T = 0.0$ and $T = 4.0$. Displayed are horizontal cross sections of the geostrophic winds on the upper boundary ($Z = 1.0$), midlevel ($Z = 0.5$), and the top of the boundary layer ($Z = 0.0$). The horizontal vector in the bottom-left corner of each vertical column corresponds to 17 m s^{-1}. The coordinate transformation given by (3.5.e)–(3.5.g) and the attendant scale contraction in cyclonic-flow regions is not included in this plot.

At $T = 0.0$, the height field on $Z = 0.0$ (not shown) has an anomaly over the model domain of 7 dam, (pressure deficit of 8.4 mb). The low-level PV disturbance produces a large-scale cyclonic gyre with maximum surface winds of approximately 0.34 (5.78 m s^{-1}). On $Z = 0.5$ (midlevel) the maximum winds are 0.66, (11.22 m s^{-1}). The upper-level PV anomaly contributes approximately 7 m s^{-1} to these winds. On $Z = 1.0$ (upper boundary) the maximum winds are 1.3 (22.1 m s^{-1}), and the upper-level PV anomaly contributes approximately 4 m s^{-1} to these winds.

At $T = 4.0$ (86 h) the height-field anomaly on $Z = 0.0$ (not shown) has increased to 20 dam (pressure deficit of 24 mb). On $Z = 0.0$ the maximum geostrophic winds increase from 0.34 to 1.35, corresponding to an increase from 5.78 m s^{-1} to 22.9 m s^{-1}. The total horizontal winds $\mathbf{u}_T = \mathbf{u}_g + \mathbf{u}_a$ (not shown) have a similar rotary structure, but the magnitudes are slightly reduced. At $T = 4.0$ the maximum total winds on $Z = 0.0$ are 1.10, or 18.7 m s^{-1}.

The strength of the horizontal winds decreases with height until very near the tropopause layer, where they increase again in association with the upper-level flow. The maximum winds on $Z = 1$ are 2.24 (38 m s^{-1}). Noteworthy features of the upper-level winds ($Z = 1$) include a pronounced anticyclonic outflow slightly downstream of the surface PV maximum, and an upper-level pressure ridge located near the upper-level outflow. Integration was terminated at $T = 4.0$, but related experiments indicate that storm intensification, and a further contraction in the radius of maximum winds, would occur at later times.

Consider the geostrophic winds on $Z = 0.0$ at $T = 4.0$. If we plot wind speed versus distance from the storm center (the center being defined by the point of minimum pressure), we find upon transforming the data back to real coordinates the radius of maximum winds contracts by 300 km, from approximately 1300 km to 1000 km (neglecting the asymmetry). Therefore, the low-level circulation in real coordinates occupies a somewhat smaller area than indicated by Fig. 3d. However, full-fledged hurricanes and even tropical storms still have a substantially smaller radius of maximum winds. Further comment regarding the simulated inner wind field structure is reserved for the conclusion.

Example 2. As a second example, consider the same initial condition as (3.6) but take $R(Z) = R_0$, with $R_0 = 0.03$, as a model for deep moist neutral saturated ascent. Development is more rapid in this case, and results are displayed in Figs. 4a–c.

Figure 4a illustrates spinup at $T = 1$ and $T = 2.83$ (21.7 and 61.6 h, respectively). The left column shows vertical cross sections of the potential vorticity Q_g, while the right column shows vertical cross sections of the absolute vorticity field. The location of the merid-

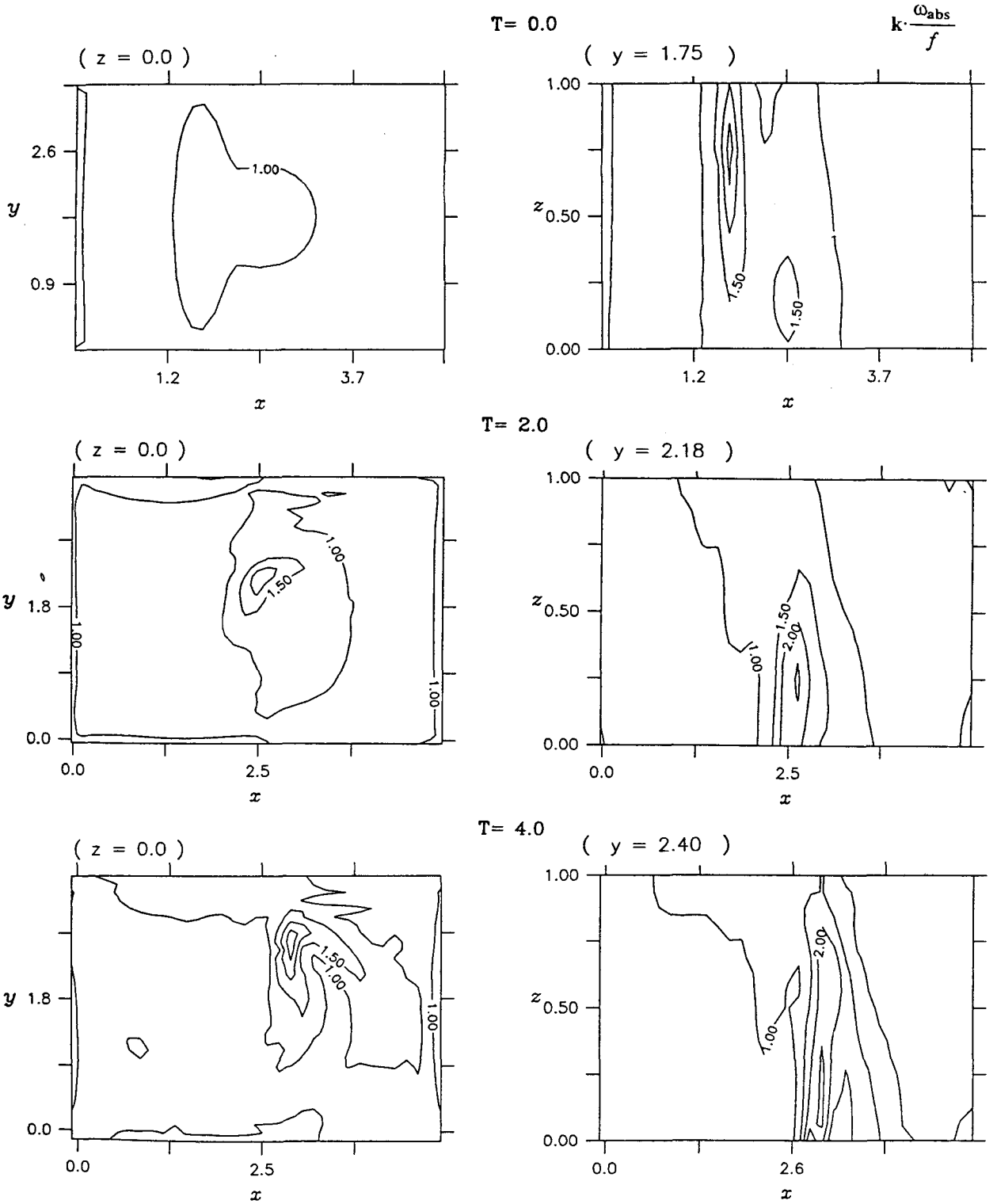

FIG. 3c. Moist 3D dynamics for example 1 (as in Fig. 3a) at $T = 0.0$, 2.0, and 4.0 (0.0, 43.5, and 87 h, respectively). Shown are contour plots of the vertical component of absolute vorticity normalized by f, $\mathbf{k} \cdot \boldsymbol{\omega}_{abs}/f$, at the top of the boundary layer $Z = 0.0$, and through the meridional cross section corresponding to the absolute vorticity maximum on $Z = 0.0$. The contour interval is fixed at 0.50. Solid lines denote positive values.

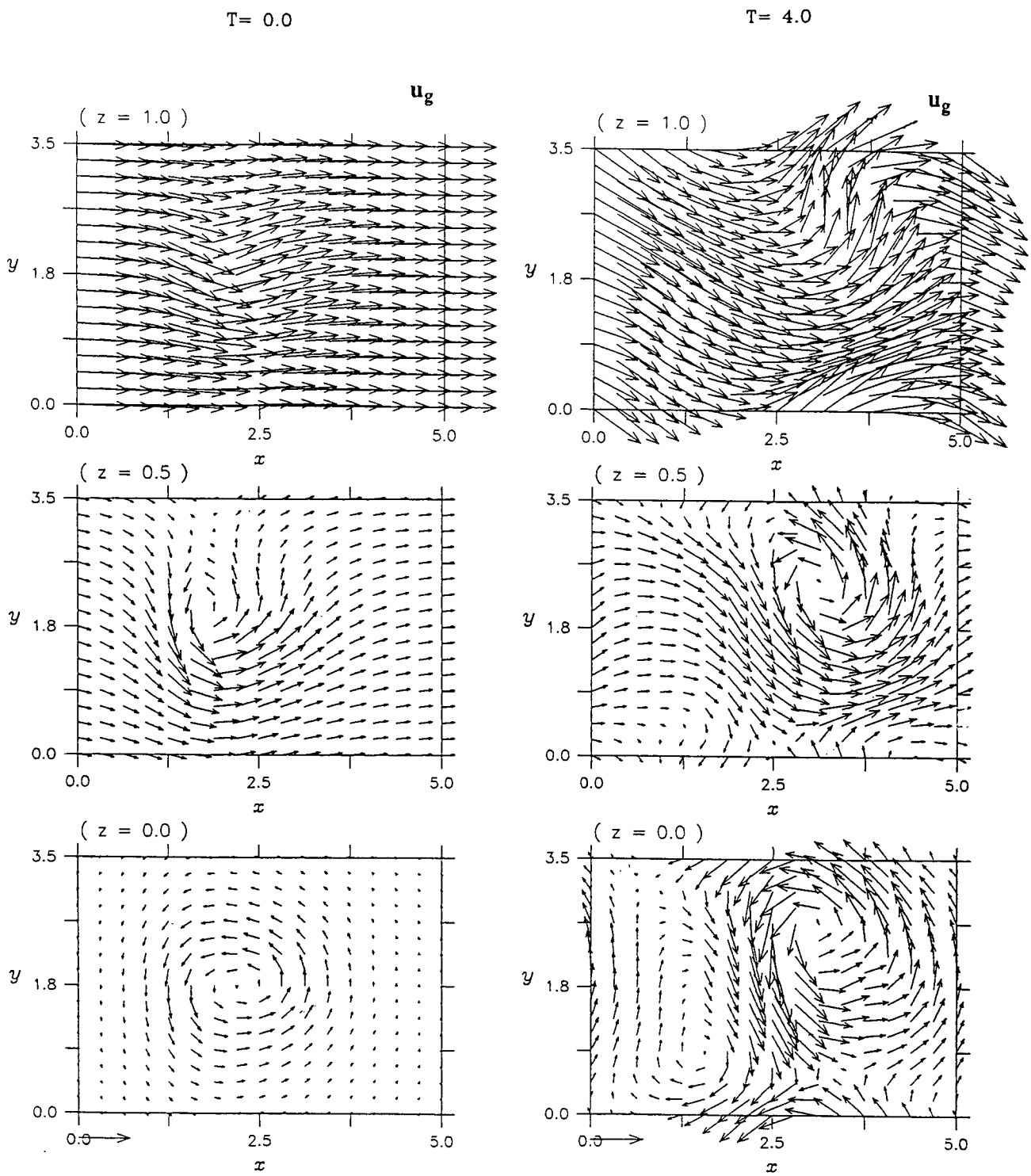

FIG. 3d. Moist 3D dynamics for example 1 (as in Fig. 3a) at $T = 0.0$, and 4.0 (0.0 and 87 h, respectively). Vector plots of the nondimensional geostrophic winds $\mathbf{u}_g$ are shown in each column. The winds on $Z = 1.0$ ($\approx$13 km), $Z = 0.5$ ($\approx$7 km), and $Z = 0.0$ ($\approx$1 km) are displayed in the upper, middle, and lower plots, respectively. The coordinate transformation back to real coordinates is not included in this plot. The horizontal vector in the bottom left corner of each column corresponds to 17 m s^{-1}.

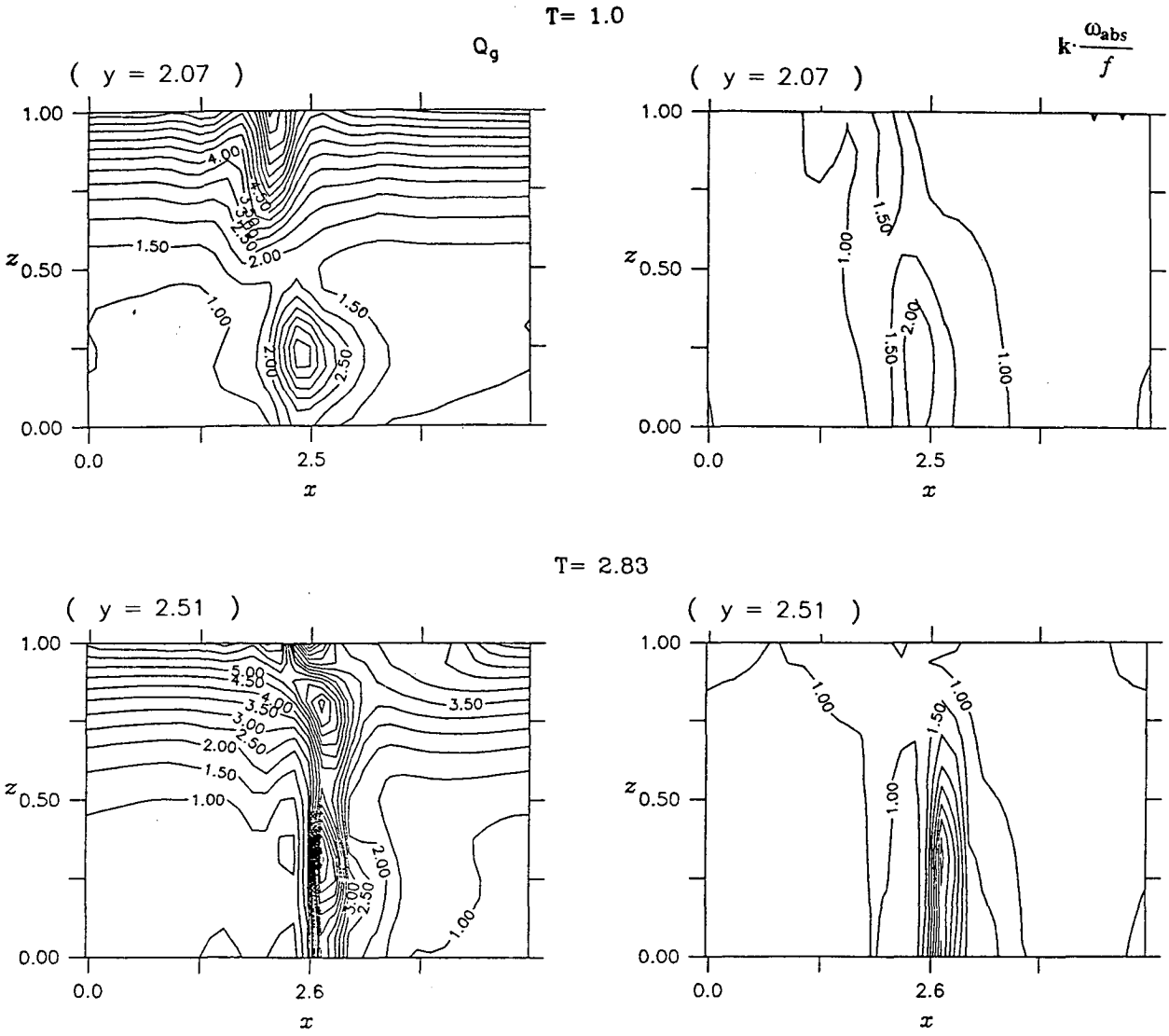

FIG. 4a. Moist 3D dynamics for example 2 assuming deep neutral ascent ($R(Z) = 0.03$) at $T = 1.0$ and 2.83 (21.78 and 61.6 h, respectively). The initial condition is given by (3.6). Shown are meridional cross sections of total PV, (Q_g), and absolute vorticity. The contour interval for both Q_g and the absolute vorticity is fixed at 0.50. Solid lines denote positive values. Unit values are the same as in Figs. 3a and 3c. One horizontal unit of distance corresponds to 1333 km.

ional cross section corresponds to the absolute vorticity maximum on $Z = 0.0$. By $T = 2.83$, a thin tube of PV and absolute vorticity extends high into the troposphere.

Figure 4b shows three horizontal plots of the total potential vorticity Q_g and the Jacobian on $Z = 1.0$, 0.50, and 0.0 at $T = 2.83$. Horizontal plots of Q_g are shown in the left column, while the right column shows horizontal contours of the absolute vorticity. The spin-up sequence is similar to that in the first example, although magnitudes of the PV and absolute vorticity are larger in this case. A striking feature is the "hole" in the PV field on $Z = 1.0$. Latent heat release has carved out a region of extremely low (negative) PV, and the uppermost portion of the initial PV anomaly has disappeared. Integration was terminated at this time, since Q_g was negative in this region (≈ -0.40), and our elliptic solver for Φ' would no longer converge. The rapid destruction of upper-level PV is consistent with observations of collapsing cold domes during tropical cyclone formation (Riehl 1979; Bosart and Bartlo 1991).

Figure 4b exhibits a small-scale cyclonic PV anomaly and absolute vorticity maximum throughout the lower to middle troposphere between $Z = 0.0$ and $Z = 0.5$. On $Z = 0.5$ there are two PV maxima. The small PV maxima lies directly over the induced surface PV, while the second maximum can be identified as the lower portion of the initial upper-level PV anomaly. For reasons discussed below, the latter PV maximum slowly

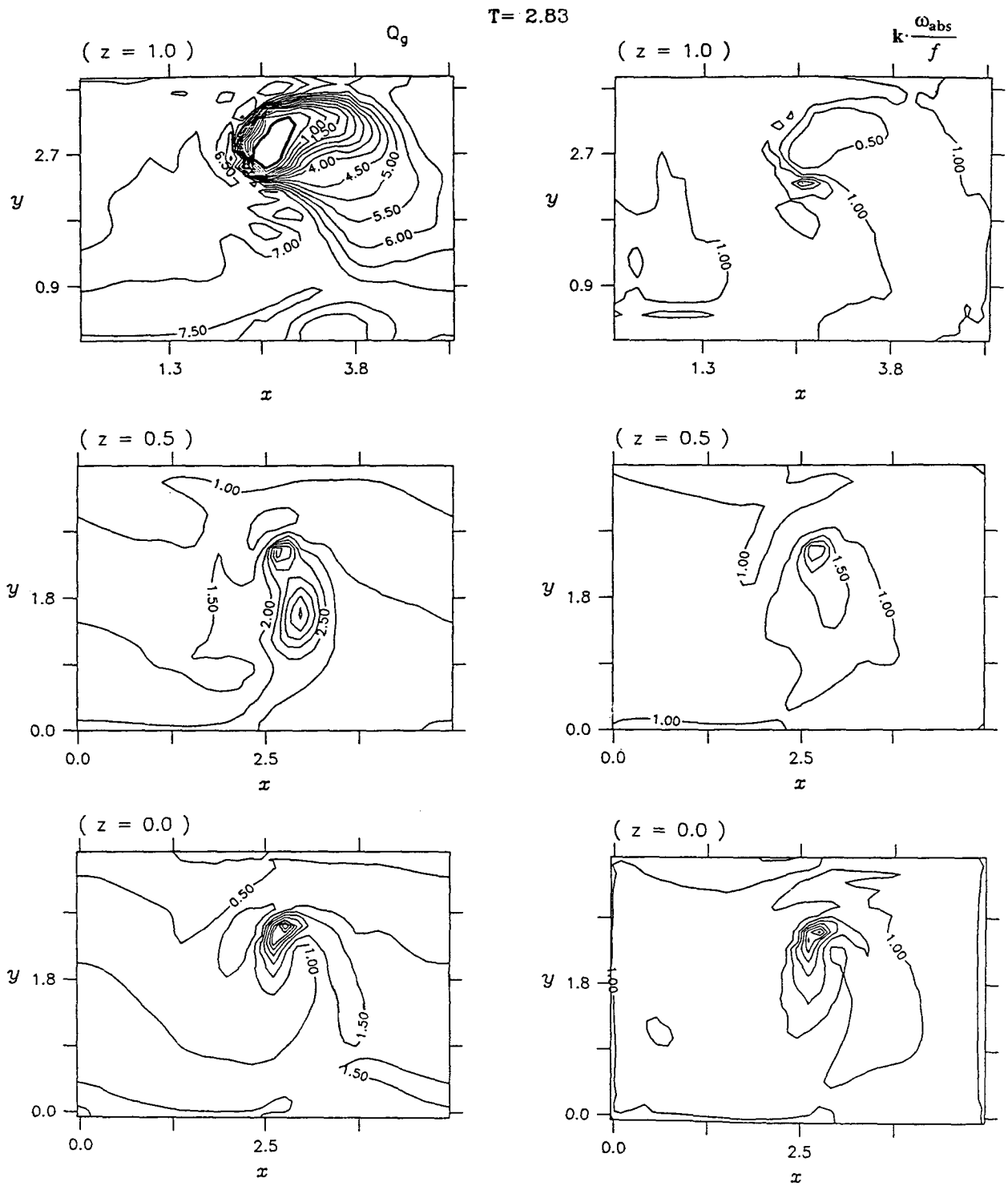

FIG. 4b. Moist 3D dynamics for example 2 assuming deep neutral ascent ($R(Z) = 0.03$) at $T = 2.83$ (61.6 h). The left column shows horizontal contour plots of total PV, (Q_g), on $Z = 1.0$, 0.5, 0.0. The right column shows horizontal contour plots of absolute vorticity. The contour interval for both Q_g and absolute vorticity is fixed at 0.50. Solid lines denote positive values, and unit values are the same as in Figs. 3a and 3c. The bold contour in the PV plot on $Z = 1.0$ indicates the zero PV contour.

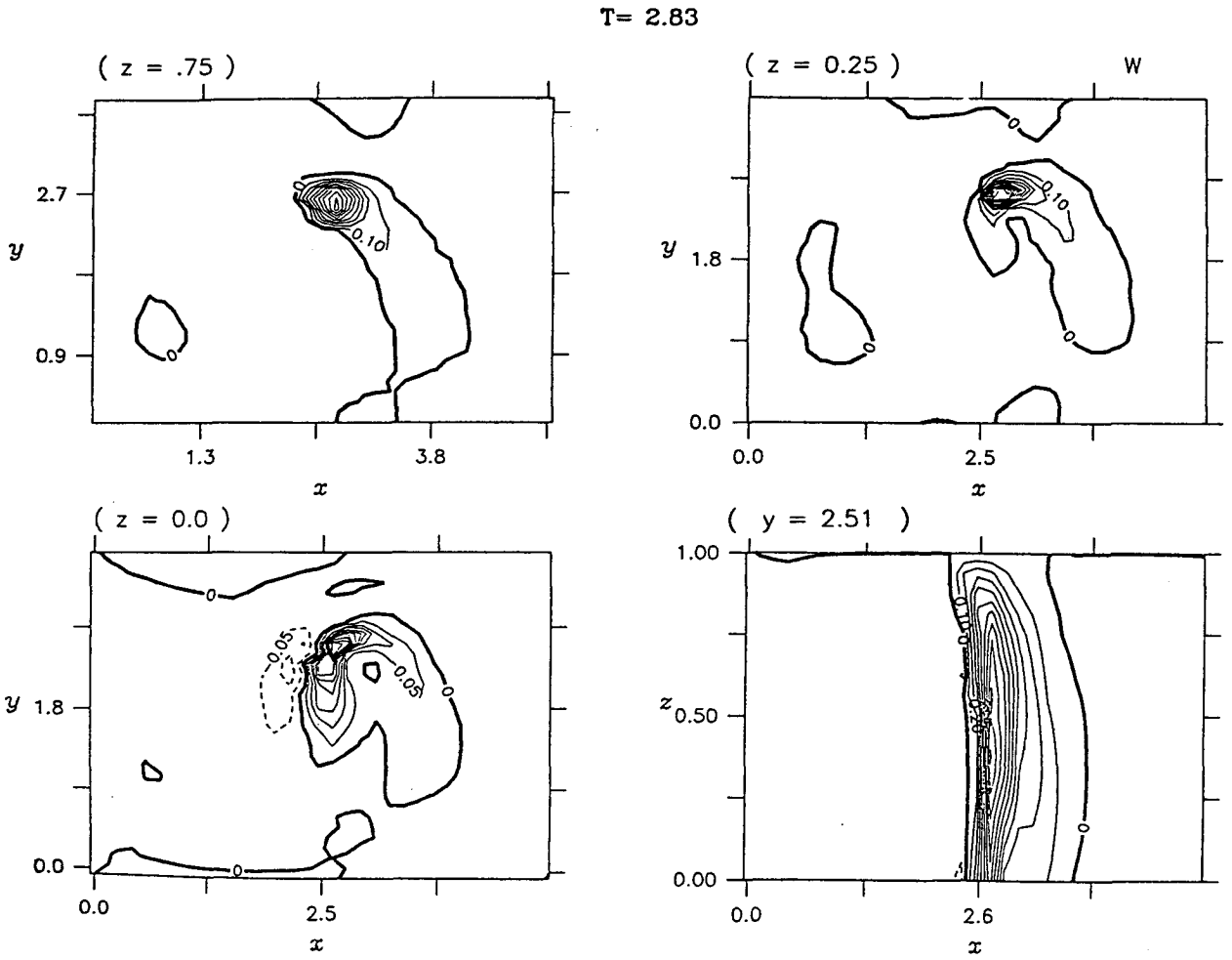

FIG. 4c. Moist 3D dynamics for example 2 assuming deep neutral ascent [$R(Z) = 0.03$] at $T = 2.83$ (61.6 h). Shown are four plots of the vertical velocity w consisting of one meridional cross section and three horizontal sections on $Z = 0.75$ ($\approx$10 km), 0.25 ($\approx$4 km), 0.0 ($\approx$1 km). The contour interval on $Z = 0.0$ is 0.05; otherwise, the contour interval is 0.10. Solid lines denote positive values, dashed lines denote negative values, and bold lines denote the zero contour. A unit value of w corresponds to 15.3 cm s^{-1}.

intensifies as it is advected around the more rapidly developing smale-scale PV tube. On $Z = 0.0$ the maximum absolute vorticity is $4.66f$, while on $Z = 1.0$ there is a pool of low absolute vorticity in the ascent region. The minimum absolute vorticity in this region is $+0.057f$, and the upper-level winds are strongly anticyclonic (not shown). Slightly south of the vorticity minimum lies a vorticity maximum associated with upper-level frontogenesis on the rigid lid.

Figure 4c shows three horizontal contour plots of the vertical velocity, w, taken at $Z = 0.75$, 0.25, and 0.0. The plot in the lower-right corner is a vertical cross section of w taken through the absolute vorticity maximum on $Z = 0.0$. Note the small tube of rising moist air extending from $Z = 0.0$ to $Z = 0.75$. The maximum vertical velocity occurs near $Z = 0.3$ with a maximum value of approximately 1.4, or 21.4 cm s^{-1}. The maximum PV and absolute vorticity are also found at this level. Magnitudes of the wind and pressure fields are similar to example 1, but the horizontal scale of the storm is slightly smaller than example 1.

Example 3. Results for dry adiabatic dynamics ($R \equiv 1.0$) are displayed in Fig. 5. The first plot is a meridional cross section of the vertical velocity at $T = 0.0$, while the second plot is a snapshot of the geostrophic winds at $T = 4.0$ (86 h). For dry dynamics, the ascent region is much shallower and wider, and the ascent velocity is approximately five times weaker than the moist case. By $T = 4.0$, the geostrophic winds on $Z = 0.0$ have only increased to 0.56, or 9.52 m s^{-1}. For dry dynamics, there is negligible spinup, and no surface PV generation as the upper anomaly is advected over the lower anomaly.

Deep saturated ascent in a moist neutral environment is essential for strong vertical coupling between upper- and lower-level PV disturbances. This is par-

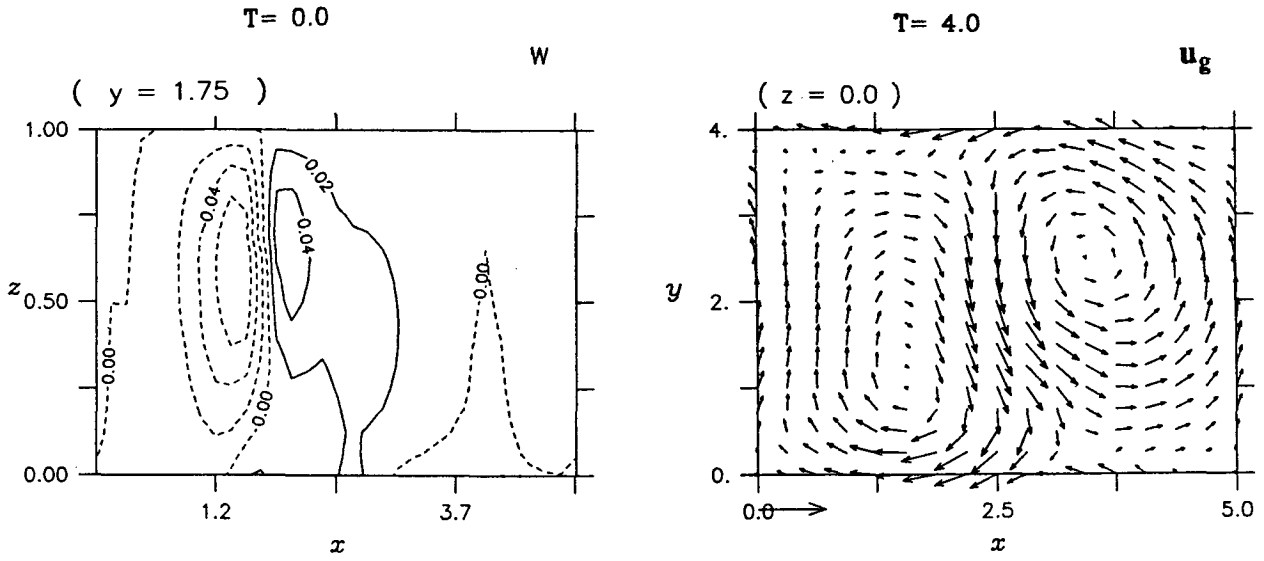

FIG. 5. Dry 3D dynamics (example 3, $R \equiv 1.0$) starting from the same initial condition (3.6) at $T = 0.0$ and $T = 4.0$ (0 and 84 h, respectively). The left figure is a meridional cross section of the vertical velocity w along $y = 1.75$ at $T = 0.0$. The right figure shows the geostrophic winds on $Z = 0.0$ at $T = 4.0$. Contour and plotting conventions are the same as in Figs. 3b and 3d.

ticularly true in the tropics where upper-level disturbances are observed to occur near the tropical tropopause, which is higher than the midlatitude tropopause. Physically, in order to maintain thermal-wind balance in the presence of a small static stability in ascent regions, stronger ascending currents are required. Strong ascent results in vortex stretching at low levels, and generation of surface PV that then augments the interaction between these systems. Thus, upper-level PV disturbances can initiate, and strongly influence, tropical cyclone formation even in instances of no surface baroclinicity and weak upper-level baroclinicity.

c. *Evolution experiments without upper-level forcing*

When we run example 1 without the upper-level PV anomaly, a much more gradual intensification ensues. After 87 h, a weak cyclone emerges possessing 10.8 m s^{-1} geostrophic surface winds and a weak upper-level anticyclone slightly downstream of the surface vortex. As discussed in previous work (MF; cf. section 3b), a localized vortex will not remain thermally balanced in a baroclinic environment without ascending and descending motions near the vortex. This remains true even in a weak baroclinic atmosphere. For moist dynamics positive low-level PV will be produced in ascending regions, and in the limit $R \to 0$ (within a sufficiently deep layer) the generation of low-level PV may offset frictional dissipation. Depending on the magnitude of R, the Ekman dissipation, δ, and the low-level baroclinicity, the surface vortex may or may not intensify.

If we reposition the low-level PV anomaly to $Z_l = 0.0$, but keep R and δ the same as in example 1, we find that the vortex slowly decays. Since the baroclinicity implied by (3.3) is smallest on $Z = 0.0$ ($\approx$900 mb), the omega response for the repositioned vortex is weaker than the experiment with it positioned at $Z_l = 0.2$ ($\approx$700 mb). In this case, the low-level PV generation is not strong enough to counteract the dissipation.

The meridional temperature gradient associated with the basic state (3.3) vanishes on $Z = 0.0$, but increases linearly with Z. Had we used a basic state with even less baroclinicity at midlevels, these experiments suggest that the slow intensification without upper-level forcing would be suppressed. Nevertheless, the basic spinup mechanism associated with upper-level forcing in moist neutral regions should not be fundamentally altered. Barring other environmental factors, these experiments also suggest that weak low-level baroclinicity can help maintain, or slowly augment, a tropical cyclone's intensity in a sustained near-moist neutral environment.

4. Discussion and conclusions

The physics of tropical cyclone formation is not well understood, and more is known about the mature hurricane structure than about the formative mechanisms that produce it. We believe part of the reason for this can be traced to insufficient upper-level atmospheric data. Given deficient upper-level observations, theories of cyclone formation focus on internal processes associated with cumulus convection and/or air–sea interaction. In this work we have instead focused on external mechanisms. Particular emphasis was placed on understanding the influence of upper-level potential vorticity disturbances on the cyclogenesis process.

In order to isolate the mechanism underlying the

interaction between upper-level potential vorticity disturbances and low-level tropical disturbances, the physically simpler model of the symmetric response to upper-level momentum driving in a two-dimensional nonlinear moist GM model was studied first. Assuming saturated ascent in a moist neutral atmosphere, thermal-wind balance implies deep ascent below the intensifying upper vortex. For chosen model parameters, low-level vortex stretching causes a rapid spinup of surface vorticity, and a dramatic scale contraction to subsynoptic scales. Latent heat release aids in the production of a deep cyclonic vortex with approximately 22 m s^{-1} surface winds. The potential vorticity is maximum in the center of the upper vortex and extends to the surface in a thin PV tube with a secondary maximum on $Z = 0.0$. In contrast, for dry dynamics, equivalent upper-level driving produces a highly localized upper-level cyclone and negligible spinup at low levels.

Three-dimensional potential vorticity dynamics in weak upper-level baroclinic zones was then explored with a three-dimensional nonlinear moist geostrophic momentum model. As an example, we considered model parameters based on the case of tropical storm Diana, which formed in September 1984 in association with an approaching elongated upper-level trough and a surface front off the northeastern coast of Florida. The model basic-state flow consists of an upper-level westerly zonal flow with 9.56 m s^{-1} winds at approximately 10 km, close to the subtropical tropopause, no motion on $Z = 0.0$, and zero surface temperature gradient. Assuming moderately deep saturated ascent in a moist neutral environment, a cyclone, possessing rotary surface winds of approximately 20 m s^{-1} (tropical storm intensity) forms in 87 h ($\approx$3.6 days). The evolution of the surface potential vorticity suggests the tendency toward a spiral structure. Integration was terminated at this time, though related experiments indicate that a further intensification would occur.

As a second example, we considered the same three-dimensional initial flow, but assumed deep saturated ascent in a moist neutral environment. Development is more rapid in this case, and a small-scale cyclone of tropical storm intensity forms in 61 h ($\approx$2.5 days). Noteworthy aspects of the vertical cyclone structure include a thin deep tube of potential vorticity and absolute vorticity that extends from upper levels down to $Z = 0.0$. Near the tropopause we find a region of very low (negative) potential vorticity, and strong anticyclonic flow in the ascent region. While these aspects were also observed in the first example, they are much more pronounced in cases associated with deep moist neutral ascent. Previous work illustrated the rapid depletion of upper-level potential vorticity in cases of deep moist neutral ascent (MF), and in the example studied here, the initial upper-level potential vorticity anomaly is annihilated during cyclogenesis. This result is consistent with observations of collapsing cold domes during the formation process (Riehl 1979; Bosart and Bartlo 1991). In this case, perhaps a more appropriate description of this process is annihilated cold domes. On the other hand, for dry dynamics there is minimal coupling between the upper- and lower-level flow, and negligible development over a comparable time interval. Thus, deep saturated ascent in a moist neutral environment is found to be essential in this model for production of strong vertical coupling between upper- and lower-level potential vorticity disturbances. These results also suggest that the formative time scale for tropical cyclones in association with upper-level forcing is sensitive to the vertical distribution of the moist stability parameter.

For simplicity, in order to isolate the upper-level forcing mechanism, we have purposely neglected additional intensification mechanisms. For example, if we were to include the effects of entrainment (as in Ooyama 1969), then we would anticipate the tendency for an enhanced midlevel radial inflow. The Coriolis force acting on this enhanced radial circulation could lead to an even stronger surface vortex. Depending upon the entrainment efficiency of the cumulus ensemble, it is possible that a more rapid spinup would result with the same forcing, or that an equivalent response would occur with even weaker forcing. This topic remains for future work.

We conclude that migratory upper-level troughs can initiate and strongly influence tropical cyclone formation, even in cases with weak upper-level shear and no surface temperature gradients. Based on these results and the aforementioned observations, we suggest the conceptual model of tropical cyclone initiation by mobile upper-level PV anomalies in areas of deep moist neutrality.

This viewpoint is similar to that of Pfeffer and Challa (1981, 1992), and Challa and Pfeffer (1980, 1990), in the sense that while most necessary conditions may be satisfied additional external forcing is believed critical in providing the necessary starting mechanism. We associate the external forcing with migratory PV anomalies in upper-level shear as the instigating agent.

Three-dimensional primitive equation (PE) models generally contain solution components from both the "slow" and "fast" manifolds. Azimuthally averaged eddy angular momentum and eddy heat fluxes computed from PE formally include contributions from fast–fast, fast–slow, and slow–slow eddy flux correlations. Observations suggest that tropical cyclogenesis may be primarily a slow manifold process driven by the balanced response to the slowly interacting upper- and lower-level PV fields. (Moist convection is obviously a fast manifold process, but we believe its representation in the slow manifold is still meaningful during genesis via the simple scheme adopted here.) Thus, while PE models are more accurate and may

suggest that the slow evolution is dominant, it is often difficult to interpret their output. Here, we have completely excised the fast (inertia–gravity and gravity wave) modes in order to capture the essence of the formation process in association with upper-level transient PV forcing. Our results lend further support to the hypothesis that tropical cyclogenesis is essentially a slow manifold phenomenon.

The Diana case motivated the parameterization of the basic-state flow and the initial upper-level PV anomaly in section 3. Diana provides an example of "subtropical developments" that typically occur north of 20° latitude in conjunction with episodic intrusions of extratropical upper-level disturbances into the subtropics (Riehl 1948). In the deep tropics, typically between 5° and 20° latitude, tropical cyclones may form by a similar process, but with weaker shears, or perhaps in conjunction with other upper-level configurations that have not been considered thus far.

Cyclogenesis in the deep tropics may also occur by altogether different mechanisms of external forcing or evolution. For example, a conceptual model recently proposed by Zehr (1991), and supported by related work of Gray (1988) and Lee et al. (1989), postulates a two-stage process comprising two pulselike events, each consisting of a low-level rotary wind surge and an associated convective burst of upward motion over a relatively large area with an attendant spinup of vorticity. While this mechanism may be different from the mechanism considered here, we note that the upper-level forcing theory is not inconsistent with such a model. Under favorable conditions, the response of a tropical cloud cluster to two or more separate interactions with upper-level cutoff PV anomalies would also promote convective bursts and low-level rotary wind surges as illustrated in section 3. Each PV interaction need not be as strong as the examples given in section 3, though the cumulative effect might produce a similar result. Clearly, more upper-level data is needed to further elucidate and identify the formative mechanisms in these regions.

Inferences from the upper-level forcing hypothesis as well as a discussion of model limitations follow.

1) *Cyclogenesis conditions.* Necessary conditions for tropical cyclone formation have been discussed in Riehl (1979; see chap. 10) and Gray (1968). One condition is that the atmosphere must be capable of permitting deep moist convection. Another is that the vertical shear of the horizontal wind be small. In this work, we assume that deep moist convection maintains a state of moist neutrality to large-scale ascent (i.e., $R \to 0$). The requirement for weak vertical shear can be partly explained with this model by noting that the strength of the upper-level winds can regulate the duration of upper-level support. If the winds aloft are so strong to advect the upper-trough over (or around) the low-level disturbance before sufficient omega coupling can occur, vortex spinup will be curtailed prematurely. For simplicity, we chose an upper-level zonal flow to illustrate the basic physics. Observations of tropical cyclogenesis, however, report varied upper-level configurations that are conducive for development (Riehl 1979; Chen and Gray 1985). Of equal interest is the problem of identifying unfavorable upper-level conditions. Understanding the influence of the upper-level flow on the formation process is an important topic for future study.

Further remarks are warranted regarding possible effects of vertical shear. Hurricane specialists indicate that when a tropical convective complex (henceforth identified with an easterly wave, cloud cluster, etc.) encounters an upper-level trough, the low-level vortex often gets decoupled from the convection, leaving behind an exposed circulation at low levels that decays with time. Such observations do not necessarily invalidate the upper-level forcing theory. Rather, they suggest that there may be a class of admissible shears and PV anomalies (i.e., strong enough to promote deep sustained ascent, yet not so strong as to significantly disrupt the cumulus environment) that interact favorably with low-level disturbances to initiate the cyclogenesis process. For simplicity in this work, we have not included a feedback between the R parameter and the local vertical shear.

2) *Scale selection.* According to this theory, the scale of the incipient vortex is set by the scale of the initial upper-level PV anomaly, the scale of the lower-level vorticity center, and the implied field of ascending motion required by thermal-wind balance. As previously noted, the deviation from moist neutrality modulates the depth and width of the ascent region, and also the strength of ascent. During intensification, ageostrophic advections cause the developing cyclone to contract in scale. Physically speaking, dissipative processes and the constraint of angular-momentum conservation ultimately terminate the scale contraction.

3) *Warm-core structure.* Condensational processes are modeled by assuming saturated entropy conservation in ascending regions and dry entropy conservation in descent regions (MF). In the moist neutral case ($R \to 0$), this model prevents changes in thermal structure within ascending regions. Adiabatic cooling is checked by condensational heating, and consequently the atmospheric column within the convective region is warmed only by horizontal advection of the thermal field. In reality, convective cells heat the atmosphere in small downdrafts adjacent to ascending buoyant plumes. This small-scale effect has not been incorporated in the present model. Large-scale subsidence within the eye of a mature hurricane produces a similar warming effect. The hurricane eye is associated with the mature tropical cyclone, but the physics of eye formation and its role in regulating storm in-

tensity is another problem. In any event, observations suggest that a warm core forms at upper levels well before the mature stage (Yanai 1968; Bosart and Bartlo 1991). Thus, while our model cyclones do not exhibit a strong warm core, we believe that the results nevertheless illustrate the essence of the formation process in association with upper-level forcing.

4) *Cyclone development and mature hurricane structure.* Is the mature hurricane primarily the result of favorable external upper-level support or purely internal processes? Numerical simulations illustrate the transformation from a finite-amplitude vortex disturbance, through tropical storm stage, to a mature hurricane by purely internal processes (Rosenthal 1978; Rotunno and Emanuel 1987; and many others). Not all tropical storms, however, reach hurricane intensity. One explanation for this is that the nondeveloping storms may move into areas of strong vertical shear, or regions of lower sea surface temperatures. On the other hand, intense polar cyclones are observed to form in regions of strong vertical shear and relatively cold sea surface temperatures, but nevertheless possess a striking similarity to the hurricane (Businger 1991). Recent work suggests the importance of external forcing in regulating hurricane intensity and structure change (Shapiro and Willoughby 1982; Holland and Merrill 1984; Molinari and Vollaro 1989, 1990). This raises the interesting hypothesis, noted also by Riehl (1979; see chap. 10, p. 468), that the transformation from a tropical storm to a mature hurricane may require continual upper-level support. The upper-level support may consist of one slowly moving upper-trough favorably located to promote deep saturated ascent, or in multiple encounters with upper-level troughs near the storm's trajectory. In addition, an auxiliary intensification mechanism, such as CISK or air–sea interaction, may be necessary for realizing the mature hurricane structure. Increased upper-level data and further modeling studies of this nature with the GM model and more accurate balance and primitive equation models should help answer this question.

5) *Cyclone prediction.* We believe that the formative stages of the tropical cyclone life cycle will remain a mystery as long as there is only limited upper-level data. Given a sufficiently dense observing network in the tropics that extends up to the tropical tropopause ($\approx$16 km), it should be possible to predict tropical cyclone formation with an accuracy comparable to predictions of midlatitude cyclones. Indeed, recent model simulations of the Pacific supertyphoon Hope using a high-resolution general circulation model suggest that hurricane forecasting is currently within reach of existing modeling technology (Krishnamurti and Oosterhof 1989). For a variety of cases, their model correctly predicts cyclone formation, but underestimates the maximum surface wind by roughly a factor of 2 (Krishnamurti et al. 1989). Their findings are consistent with our belief that large-scale models may be useful for predicting cyclogenesis, even though they may not resolve every detailed feature of the cyclone core.

We hypothesize that the formative mechanism for many tropical cyclones is, in fact, similar to the formative mechanism for midlatitude cyclones, but with the condensation process and deep moist convection playing a more essential role in the tropical case. We believe that cyclone formation in the earth's atmosphere may be fundamentally unified based on transient development theory within a balanced model framework appropriately modified to include the effects of convection.

Acknowledgments. This work was supported by NSF ATM-8912432 and by an appointment to the Global Change Distinguished Postdoctoral Fellowships sponsored by the U.S. Department of Energy, Office of Health and Environmental Research, and administered by Oak Ridge Associated Universities. We would like to thank Dr. Allan Robinson for providing plotting resources. Dr. Donald Anderson lent advice on numerical methods. Insightful conversations with Mr. Dan Reilly, Dr. Mark Handel, Dr. Lloyd Shapiro, Dr. Katsuyuki Ooyama, and Dr. Wayne Schubert are acknowledged. Numerical computations were supported by NCAR SCD 35121031, and we express our appreciation to the SCD consulting staff for their assistance in using the CRAY Y-MP 8/864. Finally, we appreciate the constructive comments of the reviewers.

APPENDIX

Summary of Numerical Method for Section 3

Details of the numerical solution to (3.4, 3.5) have been described elsewhere in Montgomery and Farrell (1992), but the non-Y periodicity of the basic-state flow requires a slight modification from previous work. For completeness, the algorithm is summarized below. The overall method is similar to previous work (MF) except we use a second-order Arakawa finite-difference scheme for the horizontal advection term (Arakawa 1966), and a fourth-order Shapiro filter on the PV field to suppress computational noise (Robinson and Walstad 1987). The elliptic equations (3.4.d) and (3.4e) are solved by SOR. The PV and boundary potential temperature are minimally corrected within each time step to ensure solvability of (3.4.d). The Jacobian term in the omega equation is evaluated after Φ' is determined from (2.3.d), and its local time derivative is approximated with an Euler difference. We also note that initial discontinuities in spatial derivatives of (3.6) on lateral boundaries are damped and do not contaminate the cyclogenesis process.

Local interactions between upper- and lower-level PV anomalies should not be strongly influenced by the horizontal boundary conditions, provided of course

that the boundaries are not too close to cyclogenesis regions. For the zonally homogeneous basic flow (3.1), we assume X periodicity for all flow variables. Meridional boundary conditions on $Y = 0$ and $Y = L_Y$ are as follows. For simplicity, we assume that Φ' and w are periodic in Y. The basic-state potential temperature $\bar{\Theta}$, however, is not periodic in Y, so we do not assume Y periodicity for $\Theta \equiv \bar{\Theta} + \Theta'$. Since (3.3) implies a gradual meridional PV gradient, Y periodicity is not assumed for Q_g.

Suppose at one instant, Θ on $Z = 0$, 1, and Q_g everywhere in $0 \leq X \leq L_X$, $0 \leq Y \leq L_Y$, and $0 \leq Z \leq 1$ are known. To update Q_g and Θ along $Y = 0$ and $Y = L_Y$ at the next instant, the second-order Arakawa approximation to the horizontal advection terms $\mathbf{u}_g \cdot \nabla_H Q_g$ and $\mathbf{u}_g \cdot \nabla_H \Theta$ requires Q_g and Θ on $Y = -DY$ and $Y = L_Y + DY$. It is convenient therefore to define $(\Phi, \mathbf{u}_g, Q_g, \Theta)$ on an extended grid extending one horizontal grid point outside the flow domain. For simplicity, we deduce Q_g on $Y = -DY$ and $Y = L_Y + DY$ by second-order extrapolation. Boundary values of Q_g are then updated by evaluating the Arakawa operator along $Y = 0$ and $Y = L_Y$. Finally, since Φ' is doubly periodic, so is Θ', and thus Θ along $Y = -DY$ and $Y = L_Y + DY$ is defined and the advection operator is readily evaluated.

In practice, the extrapolation method for Q_g on meridional boundaries produces slight incompatibilities with the doubly periodic geopotential disturbance Φ'. In the course of a numerical integration, spurious grid-point errors in the absolute vorticity (J) and the PV fields emerge on $Y = 0$ and $Y = L_Y$, which slowly propagate into the interior domain at later times. After some finite time (typically by $T = 4$, or 87 h), these errors begin to influence the outer circulation of the model cyclones, though in every case investigated here interior development was not disrupted. Therefore, we believe this effect to be a nonphysical artifact of our choice of meridional boundary conditions. These spurious errors are eliminated by applying a weak diffusive filter to J at each time step given by

$$J^{\text{filter}} = J + \alpha \tanh\left(\frac{J}{2}\right)\left(1 - \frac{2Y}{L_y}\right)^6 \times (1 - \sqrt{Z})[\textstyle\sum J - 4J],$$

where $\sum J \equiv J_{i+1,j,k} + J_{i-1,j,k} + J_{i,j+1,k} + J_{i,j-1,k}$, and (i, j, k) denotes the X, Y, and Z grid locations, respectively. The filter is strongest on the north–south boundaries ($Y = 0$ and $Y = L_Y$), and diminishes to zero in the model interior. After each application of the filter, the PV is adjusted via

$$Q_g^{\text{filter}} = \left(\frac{J^{\text{filter}}}{J}\right) Q_g$$

to prevent the generation of unwanted sources and sinks of potential vorticity. For small α, typically on the order of 0.05, the total mass-weighted potential vorticity stayed very near constant for the duration of all numerical integrations discussed in section 3. For the first example, we chose $\alpha = 0.02$, while for the second and third examples we used $\alpha = 0.05$. Computational results are virtually identical to results without the filter, except that minimal boundary noise is eliminated.

REFERENCES

Arakawa, A., 1966: Computational design for long-term numerical integration of the equations of fluid motion: Two-dimensional incompressible flow. Part I. *J. Comput. Phys.*, **1**, 119–143.

Bosart, L., and J. Bartlo, 1991: Tropical storm formation in a baroclinic environment. *Mon. Wea. Rev.*, **119**, 1979–2013.

Businger, S., 1991: Arctic hurricanes. *Amer. Sci.*, **79**, 18–33.

Challa, M., and R. Pfeffer, 1980: Effects of eddy fluxes of angular momentum on model hurricane development. *J. Atmos. Sci.*, **37**, 1603–1618.

——, and ——, 1990: Formation of Atlantic hurricanes from cloud clusters and depressions. *J. Atmos. Sci.*, **47**, 909–927.

Charney, J., and A. Eliassen, 1964: On the growth of the hurricane depression. *J. Atmos. Sci.*, **21**, 68–75.

Chen, L. S., and W. M. Gray, 1985: Global view of the upper-level outflow patterns associated with tropical cyclone intensity change during FGGE. Colorado State University Dept. of Atmos. Sci. Paper No. 392, 126 pp.

Davidson, N. E., G. J. Holland, J. L. McBride, and T. D. Keenan, 1990: On the formation of tropical cyclones Irma and Jason. *Mon. Wea. Rev.*, **118**, 1981–2000.

Davis, C., and K. Emanuel, 1990: Potential vorticity diagnostics of cyclogenesis. *Mon. Wea. Rev.*, **119**, 1929–1952.

Eliassen, A., 1951: Slow thermally or frictionally controlled meridional circulation in a circular vortex. *Astrophys. Norv.*, **5**, 19–60.

——, and E. Kleinschmidt, 1957: Dynamic meteorology. *Handbuch der Physik*, Springer Verlag, 1–154.

Elsberry, R. L., 1987: Tropical cyclone motion. *A Global View of Tropical Cyclones*, R. L. Elsberry, W. M. Frank, G. J. Holland, J. D. Jarrell, and R. L. Southern, Eds., ONR Marine Meteorology Program, 185 pp.

——, and R. F. Abbey, Jr., 1991: Recent advances in understanding tropical cyclone motion. Naval Post Graduate School Interim Report for the Office of Naval Research, Code 1122MM, 92 pp.

Emanuel, K., 1991: The finite-amplitude nature of tropical cyclogenesis. *J. Atmos. Sci.*, **46**, 3431–3456.

Erickson, C. O., 1967: Some aspects of the development of Hurricane Dorothy. *Mon. Wea. Rev.*, **95**, 121–130.

Farrell, B. F., 1982: The initial growth of disturbances in a baroclinic flow. *J. Atmos. Sci.*, **39**, 1663–1686.

——, 1984: Modal and nonmodal baroclinic waves. *J. Atmos. Sci.*, **41**, 668–673.

——, 1985: Transient growth of damped baroclinic waves. *J. Atmos. Sci.*, **42**, 2718–2727.

Frank, W. M., 1987: Tropical cyclone formation. *A Global View of Tropical Cyclones*, R. L. Elsberry, W. M. Frank, G. J. Holland, J. D. Jarrell, and R. L. Southern, Eds., ONR Marine Meteorology Program, 185 pp.

Gill, A. E., 1982: *Atmosphere-Ocean Dynamics*. Academic Press, 662 pp.

Gray, W. M., 1968: Global view of the origin of the tropical disturbances and storms. *Mon. Wea. Rev.*, **96**, 669–700.

——, 1988: Environmental influences on tropical cyclones. *Aust. Meteor. Mag.*, **36**, 127–139.

Handel, M. D., 1990: Tropical cyclone intensification from finite

amplitude disturbances. Ph.D. thesis, Massachusetts Institute of Technology.

Haque, S. M. A., 1952: The initiation of cyclonic circulation in a vertically unstable stagnant air mass. *Quart. J. Roy. Meteor. Soc.*, **78,** 394–406.

Hawkins, H., and D. Rubsam, 1968: Hurricane Hilda, 1964. 1: Genesis, as revealed by satellite photographs, conventional and aircraft data. *Mon. Wea. Rev.*, **96,** 428–452.

Heckley, W. A., and B. J. Hoskins, 1982: Baroclinic waves and frontogenesis in a non-uniform potential vorticity semi-geostrophic model. *J. Atmos. Sci.*, **39,** 1999–2016.

Holland, G., and R. Merrill, 1984: On the dynamics of tropical cyclone structural changes. *Quart. J. Roy. Meteor. Soc.*, **110,** 723–745.

Hoskins, B. J., 1975: The geostrophic momentum approximation and the semi-geostrophic equations. *J. Atmos. Sci.*, **32,** 233–242.

——, 1976: Baroclinic waves and frontogenesis. Part I: Introduction and Eady waves. *Quart. J. Roy. Meteor. Soc.*, **102,** 103–122.

——, and I. Draghici, 1977: The forcing of ageostrophic motion according to the semi-geostrophic equations and in an isentropic coordinate model. *J. Atmos. Sci.*, **29,** 11–37.

——, M. E. McIntyre, and A. W. Robertson, 1985: On the use and significance of potential vorticity maps. *Quart. J. Roy. Meteor. Soc.*, **111,** 877–946.

Krishnamurti, T. N., and D. Oosterhof, 1989: Prediction of the life cycle of a supertyphoon with a high-resolution global model. *Bull. Amer. Meteor. Soc.*, **70,** 1218–1230.

——, ——, and N. Dignon, 1989: Hurricane prediction with a high resolution global model. *Mon. Wea. Rev.*, **117,** 631–669.

Lilly, D. K., 1960: On the theory of disturbances in a conditionally unstable atmosphere. *Mon. Wea. Rev.*, **88,** 1–17.

Lee, C., R. Edson, and W. M. Gray, 1989: Some large scale characteristics associated with tropical cyclone development in the north Indian Ocean during FGGE. *Mon. Wea. Rev.*, **117,** 407–426.

Molinari, J., and D. Vollaro, 1989: External influences on hurricane intensity. Part I: Outflow layer eddy angular momentum fluxes. *J. Atmos. Sci.*, **46,** 1093–1105.

——, and ——, 1990: External influences on hurricane intensity. Part II: Vertical structure and response of the hurricane vortex. *J. Atmos. Sci.*, **47,** 1902–1918.

Montgomery, M., 1990: Potential vorticity and diabatic processes in frontal dynamics. Ph.D. thesis, Harvard University.

——, and B. Farrell, 1990: Dry surface frontogenesis arising from interior potential vorticity perturbations in a semi-geostrophic model. *J. Atmos. Sci.*, **47,** 2837–2852.

——, and ——, 1991: Moist surface frontogenesis associated with interior potential vorticity anomalies in a semigeostrophic model. *J. Atmos. Sci.*, **48,** 343–367.

——, and ——, 1992: Polar low dynamics. *J. Atmos. Sci.*, **49,** 2484–2505.

Ooyama, K., 1964: A dynamical model for the study of tropical cyclone development. *Tech. Conf. on Hurricanes and Tropical Meteorology,* Mexico, Amer. Meteor. Soc., 187–198.

——, 1969: Numerical simulation of the life cycle of tropical cyclones. *J. Atmos. Sci.*, **26,** 3–40.

——, 1982: Conceptual evolution of the theory and modeling of the tropical cyclone. *J. Meteor. Soc. Japan,* **60,** 369–380.

Palmen, E., and C. W. Newton, 1969: *Atmospheric Circulation Systems.* Academic Press, 603 pp.

Pederson, T. S., 1991: A comparison of the free ride and CISK assumptions. *J. Atmos. Sci.*, **48,** 1813–1821.

——, and E. Rasmussen, 1985: On the cut-off problem in linear cisk models. *Tellus,* **37A,** 394–402.

Pfeffer, R., 1955: A discussion of the balance of angular momentum in hurricanes. *Bull. Amer. Meteor. Soc.*, **37,** 234.

——, 1958: Concerning the mechanics of hurricanes. *J. Meteor.*, **15,** 113–120.

——, and M. Challa, 1981: A numerical study of the role of eddy fluxes of momentum in the development of Atlantic hurricanes. *J. Atmos. Sci.*, **38,** 2393–2398.

——, and ——, 1992: The role of environmental asymmetries in Atlantic hurricane formation. *J. Atmos. Sci.*, **49,** 1051–1059.

Reilly, D., and K. Emanuel, 1991: Evidence of upper tropospheric triggering of tropical cyclogenesis. *Extended Abstracts of 19th Conf. on Hurricanes and Tropical Meteorology,* Miami, Amer. Meteor. Soc., 202–205.

Riehl, H., 1948: On the formation of west Atlantic hurricanes. Studies of Upper-Air Conditions in Low Latitudes, Victor P. Starr, Ed., University of Chicago Department of Meteorology, Victor P. Starr, Ed., Misc. Rep. No. 24, 67 pp.

——, 1979: *Climate and Weather in the Tropics.* Academic Press, 611 pp.

——, and K. Emanuel, 1991: Evidence of upper tropospheric triggering of tropical cyclogenesis. *Extended Abstracts,* of *19th Conf. on Hurricanes and Tropical Meteorology,* Miami, Amer. Meteor. Soc., 202–205.

Robinson, A. R., and L. J. Walstad, 1987: The Harvard open ocean model: Calibration and application to dynamical processes, forecasting, and data assimilation studies. *Appl. Num. Math.*, **3,** 89–131.

Rosenthal, S., 1978: Numerical simulation of tropical cyclone development with latent heat release by the resolvable scales. I: Model description and preliminary results. *J. Atmos. Sci.*, **35,** 258–271.

Rotunno, R., and K. Emanuel, 1987: An air–sea interaction theory for tropical cyclones. Part II: Evolutionary study using a nonhydrostatic axisymmetric model. *J. Atmos. Sci.*, **44,** 542–561.

Sadler, J. C., 1978: Mid-season typhoon development and intensity change and the tropical upper tropospheric trough. *Mon. Wea. Rev.*, **106,** 1137–1152.

Schubert, W. H., and J. J. Hack, 1983: Transformed Eliassen Balanced Vortex Model. *J. Atmos. Sci.*, **40,** 1571–1583.

——, and B. T. Alworth, 1987: Evolution of potential vorticity in tropical cyclones. *Quart. J. Roy. Meteor. Soc.*, **113,** 147–162.

——, P. E. Ciesielski, D. E. Stevens, and H. C. Kuo, 1991: Potential vorticity modeling of the ITCZ and the Hadley circulation. *J. Atmos. Sci.*, **48,** 1493–1509.

Shapiro, L., and H. Willoughby, 1982: The response of balanced hurricanes to local sources of heat and momentum. *J. Atmos. Sci.*, **39,** 378–394.

Shapiro, M. A., L. S. Fedor, and T. Hampel, 1987: Research aircraft measurements of a polar low over the Norwegian Sea. *Tellus,* **39A,** 272–306.

Shi, J., S. W. Chang, and S. Raman, 1990: A numerical study of the outflow layer of tropical cyclones. *J. Atmos. Sci.*, **118,** 2042–2055.

Snyder, C., W. Skamarock, and R. Rotunno, 1991: A comparison of primitive equation and semigeostrophic simulations of baroclinic waves. *J. Atmos. Sci.*, **48,** 2179–2194.

Thorncroft, C. D., and B. J. Hoskins, 1990: Frontal cyclogenesis. *J. Atmos. Sci.*, **47,** 2317–2336.

Thorpe, A. J., 1985: Diagnosis of balanced vortex structure using potential vorticity. *J. Atmos. Sci.*, **42,** 397–406.

Whitaker, J. S., L. W. Uccellini, and K. F. Brill, 1988: A model-based diagnostic study of the rapid development phase of the Presidents' Day cyclone. *Mon. Wea. Rev.*, **116,** 2337–2365.

Yanai, M., 1968: Evolution of a tropical disturbance in the Caribbean Sea region. *J. Meteor. Soc. Japan,* **46,** 86–108.

Zehr, R. M., 1991: Tropical cyclogenesis in the western North Pacific. Ph.D. thesis, Colorado State University.